GEOMETRY BASED HAND VEIN BIOMETRY

by

Pınar Sağlam

B.S., Computer Engineering, Bahçeşehir University, 2008

Submitted to the Institute for Graduate Studies in
Science and Engineering in partial fulfillment of
the requirements for the degree of
Master of Science

Graduate Program in Computer Engineering

Boğaziçi University

2012

GEOMETRY BASED HAND VEIN BIOMETRY

APPROVED BY:

Prof. Lale Akarun (Thesis Supervisor)	.....
Prof. Bülent Sankur	.....
Albert Ali Salah, Ph.D.	.....

DATE OF APPROVAL: 16.04.2012

ACKNOWLEDGEMENTS

First and foremost, I would like to offer my deepest gratitude to my thesis advisor Prof. Lale Akarun. Without her guidance and patience, this thesis would not be complete.

I also would like to thank my friends and colleagues in MediaLab and PILAB, namely, Neşe Alyüz, Yunus Emre Kara, Alp Kındıroğlu, Cem Keskin, Furkan Kıraç, Hamdi Dibeklioğlu, Heysem Kaya, İsmail Arı, Türkan Hamzaoğlu, and Umut Konur for providing a fun working environment and keeping up with me.

I thank all my friends in the computer engineering department that have helped me raise my spirits in times of bad.

I would like to offer my deepest gratitude to my parents Müzeyyen Sağlam and Ahmet Sağlam, and my brother İbrahim Sağlam. Without the support and encouragement of my family throughout my educational life I would not have been the person that I am today.

Lastly, I would like to express my deepest gratitude to my spouse İlter Karaçay who has always been there in times of need. Without his support, motivation, and patience, I could not bear the burden.

Morever, I gratefully acknowledge financial support of TUBITAK via a TUBITAK-BIDEB fellowship.

ABSTRACT

GEOMETRY BASED HAND VEIN BIOMETRY

This thesis documents a study in which new algorithms are developed for geometry based hand vein biometry. Hand vein patterns are assumed not to change over time except in their size, and they are unique to each individual, hence researchers aim to construct a biometric control system based on hand vein patterns. The approach proposed here is using free-posture captured near infrared hand vein images for both enrollment and test. We utilize Gabor filters banks to enhance the visibility of hand vein segments which is a new thing in hand vein biometry literature. Furthermore, it is robust against wrongly aligned hand vein features. The region of interests (ROIs) are extracted from hand vein images. In order to increase the visibility of hand veins in these ROIs, Gabor filter bank approach is applied. Enhanced ROIs facilitate to extract vein line segments as geometric features. To extract these line segments; thresholding, skeletonization and line edge map (LEM) extraction methods are applied on enhanced ROIs, respectively. These methods yield the LEM and the graph version of a hand vein structure. Before identity matching, a preprocessing stage is configured to alleviate the effects of wrong registrations. There are two different methods for alignment correction. The first one is based on keypoint matching, whereas the other is based on translating the compared LEMs iteratively. Last but not least, identity matching is done by several distance measurement metrics, namely, line segment Hausdorff distance (LHD), weighted line segment Hausdorff distance (WLHD), modified line segment Hausdorff distance (MLHD) and graph edit distance (GED). WLHD and MLHD are different versions of LHD, that we specialized for hand vein biometry. Additionally, an algorithm is developed to make a measurement on Graph Edit Instance (GED) metric. GED is defined as the least cost graph edit operation sequence which is used to transform one graph to another. By examining each metric, we notice that line segment matching based methods give more promising results than graph matching.

ÖZET

GEOMETRİYE DAYALI EL DAMAR BİYOMETRİSİ

Bir insana ait el damarlarının yapısının boyu dışındaki özelliklerinin zamanla değişmeyişi ve kişiye özgü oluşu, el damar verilerine dayalı biyometrik tanıma sistemleri kurma fikrinin ortaya atılmasını sağlamıştır. Bu tezde el damar verilerinin geometrisine dayalı biyometrik tanıma sistemlerinde kullanılmak üzere, yeni algoritmalar oluşturulmuştur. Yaklaşım, kayıtlı imgeler ve test imgeleri olarak herhangi bir kısıtlama olmadan, doğal pozlarında, yakın kızılberisi bantlarda kaydedilmiş el damar imgelerini kullanmaktadır. İmgelerdeki damar verilerinin görünürlüğünü arttırmak için Gabor filtre bankasından yararlanılmıştır. Gabor filtre bankasının bu amaç için kullanılışı, el damar biyometrisinde bir yeniliktir. Dahası, yaklaşımımız yanlış çakıştırılmış el damar özniteliklerine karşı gürbüzdür. Sistemimiz öncelikle el damar imgelerinden ilgi bölgesini çıkartır. Bu bölgeye Gabor filtre bankası uygulanarak ilgili bölgedeki damarlar daha da görünür hale getirilir. Geliştirilmiş ilgili bölge üzerine eşikleme, iskelet çıkartma ve Çizgi Kenar Haritası (LEM) çıkarma yöntemleri uygulanarak, damar yapısı LEM ve çizgeye dönüştürülür. Kimlik eşleştirmesinden önce, hatalı kayıtlamanın LEM üzerindeki etkilerini gidermek için tercihi iki farklı hizalama yöntemi kullanılır. Bunlardan biri ana nokta eşleştirmesine, diğeri ise yinelemeli LEM aktarımına dayanmaktadır. Kimlik eşleştirmesi için çeşitli benzerlik puanı ölçme metrikleri kullanılmıştır. Bunlar Çizgi Hausdorff Mesafesi (LHD), Ağırlıklı Çizgi Hausdorff Mesafesi (WLHD), Değişitirilmiş Çizgi Hausdorff Mesafesi (MLHD) ve Çizge Düzenleme Uzaklığı (GED)'dir. WLHD ve MLHD, LHD metriğinin düzenlenmesi sonucu el damar verilerinde kullanılmak üzere özelleştirdiğimiz metriklerdir. GED metriğine dayalı hesaplama yapabilmej için bir algoritma geliştirilmiştir. GED, incelenen çizgenin model çizgeye benzemesi için üzerinde yapmamız gereken en az maliyetteki değişikliğe verilen isimdir. Yaptığımız deneyler, çizgi mesafesine dayalı metriklerin, GED'ye göre daha iyi sonuçlar verdiğini göstermektedir.

TABLE OF CONTENTS

ACKNOWLEDGEMENTS . . . iii
ABSTRACT . . . iv
ÖZET . . . v
LIST OF FIGURES . . . ix
LIST OF TABLES . . . xii
LIST OF SYMBOLS . . . xiv
LIST OF ACRONYMS/ABBREVIATIONS . . . xv
1. INTRODUCTION . . . 1
1.1. Motivation . . . 2
1.2. Outline . . . 3
2. HAND VEIN BIOMETRY . . . 4
2.1. Modeling The Architecture of A Hand Vein Recognition System . . . 5
2.1.1. Image Acquisition . . . 5
2.1.1.1. Variations on Image Capturing Devices . . . 6
2.1.1.2. Other Variations . . . 8
2.1.2. Region of Interest (ROI) Determination . . . 8
2.1.3. Image Preprocessing . . . 9
2.1.4. Feature Extraction . . . 9
2.1.4.1. Feature Matching . . . 11
2.2. Comparative Summary of Prior Works . . . 12
3. GEOMETRY BASED HAND VEIN BIOMETRY . . . 19
3.1. Outline of the System . . . 19
3.2. Hand Normalization and ROI Extraction . . . 20
3.2.1. Yoruk Algorithm . . . 20
3.2.2. Warping Hand Segments by Thin Plate Spline . . . 22
3.2.2.1. Thin Plate Spline (TPS) . . . 23
3.2.2.2. Applying TPS to hand vein ROIs . . . 25
3.2.3. Enhancing ROIs by mean intensity value . . . 26
3.3. Feature Extraction via a Geometry based Method . . . 29

3.3.1. Gabor Filtering 30
3.3.2. Even-symmetric Gabor Filters 31
3.3.2.1. Even-symmetric Gabor filters bank construction and parameter selection 31
3.3.2.2. Hand Vein Enhancement 34
3.3.3. Geometric Representation of Hand Veins 35
3.3.3.1. Yasuda adaptive thresholding method 35
3.3.3.2. Skeletonization 36
3.3.3.3. Graph definition through Line Edge Map (LEM) . . . 37
3.4. Identity Matching 38
3.4.1. Preprocessing Stages 38
3.4.2. Optional Preprocessing 1: Enhancing registration with keypoints 39
3.4.2.1. SURF: Speeded-up Robust Features 39
3.4.2.2. Procrustes Analysis 40
3.4.2.3. Aligning two ROIs by using SURF and Procrustes Analysis 41
3.4.3. Optional Preprocessing 2: Enhancing Registration by Iterative LEM 42
3.4.4. Line Segment Hausdorff Distance (LHD) 43
3.4.5. Modified Line Segment Hausdorff Distance (MLHD) 44
3.4.6. Weighted Line Segment Hausdorff Distance (WLHD) 44
3.4.7. Graph Edit Distance (GED) 46
3.4.7.1. GED in Biometric Verification 47
3.4.7.2. Seed Node Substitution Method 48
3.4.7.3. Calculated GED through Simplified graphs G and G' . 49
3.4.7.4. Demonstration of the GED Algorithm on an Example 49
4. EXPERIMENTS 61
4.1. Dataset 61
4.2. Methodology 63
4.2.1. Recognition, Identification and Verification 63
4.2.2. Performance Measures 64
4.2.2.1. Identification Rate (IR) 64

4.2.2.2. Equal Error Rate (EER) 64
4.3. Experimental Setup 64
4.3.1. Enrollment and Test Sets 64
4.3.1.1. Experiment 1: Registration by warping 65
4.3.1.2. Experiment 2: ROI Enhancement 68
4.3.1.3. Experiment 3: Weighted LHD 69
4.3.1.4. Experiment 4: Iterative LEM 71
4.3.1.5. Experiment 5: Keypoints 75
4.3.1.6. Experiment 6: Matching by GED 80
4.3.1.7. Conclusion 81
5. CONCLUSIONS 83
5.1. Conclusion and Future Work 83
REFERENCES 91

LIST OF FIGURES

Figure 2.1. A typical architecture of a hand vein recognition system. 14

Figure 2.2. Dorsal venous network of the hand. 15

Figure 2.3. Examples of thermal indoor and outdoor images. 15

Figure 2.4. Examples of NIR images of the back of a hand with hair and no-hair. 16

Figure 2.5. Configuration of reflection and translation based hand vein image acquisition methods. 16

Figure 2.6. Examples of a relaxed and a clenched fist hand position in a hand vein image. 17

Figure 2.7. ROI determination based on finding knuckle tips and finger valleys as key points. 18

Figure 3.1. The steps of our dorsal hand vein biometry system. 19

Figure 3.2. Processing steps for hand normalization. 22

Figure 3.3. Two ROIs belong to the same person. 23

Figure 3.4. Finger valleys of a hand. 26

Figure 3.5. Two ROIs belong to the same person before and after warping. . . 27

Figure 3.6. Examples of ROIs. 28

Figure 3.7. The flowchart of ROI enhancement method. 52

Figure 3.8. Parameters of the Gabor kernel as reflected in the half-magnitude elliptic profile in frequency domain. 53

Figure 3.9. 2D spatial filters of Yang *et al.*'s even-symmetric Gabor bank and their convolution results. 54

Figure 3.10. 2D spatial filters of our proposed even-symmetric Gabor bank and their convolution results. 55

Figure 3.11. Enhanced vein images yielded by Yang *et al.*'s Gabor filters bank and our proposed Gabor filters bank. 56

Figure 3.12. Skeletonization of vein segments by "skel" option and "thin" options. 56

Figure 3.13. Feature extraction steps. 57

Figure 3.14. Three steps of Procrustes analysis. 58

Figure 3.15. $d_{\parallel}(m_i^l, t_j^l)$ and $d_{\perp}(m_i^l, t_j^l)$ dissimilarity measurements. 59

Figure 3.16. MHLD conditions in which parallel distance is accepted as 0. . . . 59

Figure 3.17. Top: graph G' bottom: graph G. 59

Figure 3.18. Changes in graph G and G' while perfoming GED algorithm. . . . 60

Figure 4.1. Camera setup of Bosphorus Hand Vein Dataset. 62

Figure 4.2. Two hand vein images captured from the same hand in which finger valleys are dissimilar. 67

Figure 4.3. Enahnced ROIs and their LEM forms constructed by different Gabor filters banks and parameters. 70

LIST OF TABLES

Table 2.1. Comparative summary of prior works on dorsal hand vein biometric field. 13

Table 3.1. The seed nodes of the graphs and calculated GED through these seed nodes. 51

Table 4.1. Dataset Information. 63

Table 4.2. Enrolment and test set pairs of single enrolment for each condition. 65

Table 4.3. Enrolment and test set pairs of double enrolment for each condition. 66

Table 4.4. MLHD measurement of warped images for single enrolment. 67

Table 4.5. MLHD measurement for single enrolment with different Gabor filters banks and LEM parameters. 68

Table 4.6. MLHD measurement for double enrolment with different Gabor filters banks and LEM parameters. 69

Table 4.7. WLHD measurement for single enrolment with different Gabor filters bank and WLHD parameter selections. 72

Table 4.8. WLHD measurement for double enrolment with different Gabor filters bank and WLHD parameter selections. 73

Table 4.9. LHD and MLHD measurements for single enrolment on iterated LEMs. 74

Table 4.10. LHD and MLHD measurements for double enrolment on iterated LEMs. 74

Table 4.11. MHLD measurement for single enrolment on aligned ROIs using SURF interest points and junctions. 76

Table 4.12. MLHD and LHD measurement for single enrolment by accepting the minimum distance of aligned and not-aligned LEMs. 77

Table 4.13. MLHD and LHD measurement for double enrolment by accepting the minimum distance of aligned and not-aligned LEMs. 78

Table 4.14. The results of using keypoint matching for object recognition for single enrolment. 79

Table 4.15. GED measurement for single enrolment with different Gabor filter banks and LEM parameters. 80

Table 4.16. The most successful results of three experiments for single enrolment are compared to literature Yuksel *et al.* [1]. 82

Table 4.17. The most successful results of three experiments for double enrolment are compared to literature Yuksel *et al.* [1]. 82

LIST OF SYMBOLS

A	Images taken after having squeezed an elastic ball repetitively (closing and opening) for one minute (Activity)
$abovecut_i$	The above cut image in the ith iteration while applying intensity based ROI enhancement method
B	Images taken after having carried a bag weighing 3 kg. for one minute (Bag)
$belowcut_i$	The below cut image in the ith iteration while applying intensity based ROI enhancement method
C	Celsius
d_θ	Angular distance between two line segments
$d_\parallel$	Parallel distance between two line segments
$d_\perp$	Perpendicular distance between two line segments
dist	Distance
$\tilde{E}$	Enhanced hand vein image with applying a Gabor filter bank
I	Images taken after having cooled image(Ice)
i	Iteration counter in intensity based ROI enhancement method
N	Images taken under normal condition(Normal)
T	Intensity based ROI enhancement threshold value
T_D	Deviation threshold of LEM algorithm
ts	Slope threshold of LEM algorithm
λ	The different cutoff wavelengths of Infrared filters

LIST OF ACRONYMS/ABBREVIATIONS

CCD	Charge-Couple Device
EER	Equal Error Rate
GED	Graph Edit Distance
ICA	Independent Component Analysis
IR	Identification Rate
LDA	Linear Discriminant Analysis
LEM	Line Edge Map
LHD	Line Segment Hausdorff Distance
MIR	Middle Infrared
MLHD	Modified Line Segment Hausdorff Distance
NIR	Near Infrared
NMF	Non-negative Matrix Factorization
PCA	Principal Component Analysis
ROI	Region of Interest
SURF	Speeded-up Robust Features
TPS	Thin Plate Spline
WLHD	Weighted Line Segment Hausdorff Distance

1. INTRODUCTION

Identity verification is needed in many real-life safety and convenience applications. Biometric recognition systems are designed to respond to the need. There exists many biometric systems that are designed to verify people on the basis of traits such as 2D or 3D face, ear, iris, fingerprint or signature data. However, each of these biometric systems has its own drawbacks. Collecting samples from ear and iris is quite difficult. To capture iris data, there is a need for expensive devices and occlusion is a very big problem for the ear. Face data are affected from aging. Fingerprint, though most reliable, also has problems as they are sensitive to wear and aging. In other words, since the current systems are indurable to changed conditions and spoof scenarios, researchers aim to develop more reliable, consistent and user friendly biometric systems. Hand vein biometry has been designed to answer these concerns.

Hand vein biometry is relatively younger than other biometric systems. For the reason that hand veins are not seen obviously under visible light, hand vein biometry requires advanced imaging devices. Owing to the developments on imaging technology, this biometry has been useful for the last two decade.

There are lots of advantages of hand vein biometry. Vein patterns are more reliable to spoofing compared to other biometrics. It is almost impossible to replicate vein segments because they lie under the skin surface and ensure liveness. Since the basic geometry of vein patterns are stable, that is, the structure of the vein patterns do not change as human beings grow older, hand vein biometry does not have aging problems. On the other hand, the visibility of the veins can be influenced from the thickness of the hand skin surface, age, physical activities, the ambient temperature or humidity. Besides, skin surface features such as spiloma, scar or hair can affect the obviousness of the vein segments. According to these issues, hand vein biometry system has to stand up to these kind of problems.

1.1. Motivation

Hand vein biometry attracts the attention of the research communities thanks to its uniqueness, stability, and strong resilience to forgery. To obtain acceptable recognition rates on a hand vein biometric system, there are many methods utilized in the literature. A hand vein biometric system consists of five stages: image acquisition, region of interest (ROI) extraction, image preprocessing, feature extraction and feature matching. These stages are described in Chapter 2 in detail. While capturing hand vein images, some factors such as skin features and ambient lighting can influence the quality of vein visibility. In the literature, the systems aim to reduce irrelevant information on hand vein image by applying noise reduction and smoothing operations. In this study, we try to enhance the visibility of vein segments on images rather than attempting to reduce noisy information.

One of the most important steps of a hand vein biometric system is extracting features from hand vein images. Hand vein feature extraction methods can be roughly split into two types as appearance based and feature based techniques. We are interested in geometry based feature extraction methods in this thesis, which consists of the spatial information of vein segments, whereas appearance based methods may use subspace-based features.

A hand vein network can be represented with lines as the result of a geometry based feature extraction method. The similarity between two hand vein images can be measured by a metric which calculates the distances between the lines of two images. In addition to this widely known geometry based feature matching technique, we use a new matching technique based on graph similarity. A hand's vein structure resembles a graph. Graph is an abstract representation of objects (vertices) where some pairs of them are connected by links (edges). In mathematics, two graphs can match only if they are exactly the same (isomorphic). However, real time applications have to be error tolerant. In order to tolerate changes on the same person's different hand vein images, we design a biometric verification method based on Graph Edit Distance (GED) metric, which modifies the graphs with node insertion, node deletion, node

substitution, edge insertion, and edge deletion operations.

1.2. Outline

The thesis is organized as follows: This chapter introduced hand vein biometry and gave the motivation to explain the underlying idea of this thesis. Chapter 2 inspects the hand vein biometry literature and gives a technical background about each step of a hand vein biometric system with reference works. In chapter 3, our biometric system and its main modules are explained and elaborated. In chapter 4, the dataset that we used in the evaluation of the methods is described. Chapter 4 also describes the experiment setup. Finally, the success rates of the experiments and analysis of these results are explained. Chapter 5 concludes this thesis with a summary of the proposed system.

2. HAND VEIN BIOMETRY

Biometrics is the use of inherent characteristics of a person for the authentication of identity. Biometrics technologies are used for security and forensic as well as human-computer interaction. DNA, face, iris, fingerprint, gait, palm print, signature, hand geometry and hand vein are among popular characteristics. Among these various biometric characteristics used for person recognition, hand-based biometrics are not only some of the oldest in the market, but also the most successful [2]. Fingerprint, palm print, knuckle print and hand geometry based biometrics are relatively older systems than hand vein since hand vein visualization is even more difficult than the former ones. Thanks to enhanced image acquisition techniques, hand vein features have been used in biometric area for the last two decades.

In general, any human characteristic could be a biometric feature if it provides the requirements of a biometric system such as universality, uniqueness, permanence, collectability and circumvention. Every human hand has a vascular structure for blood circulation that supplies universality criteria. Many resources claim that hand vein pattern has a unique property for each individual, even for identical twins [3] [4]. Besides, for a healthy human being, vein pattern does not change, but stays permanent throughout life, except in size. Owing to advanced imaging techniques it is easy to collect hand vein data. The hand vein pattern consists of subcutaneous blood vessels. Since the blood vessels are underneath the skin and also ensures liveness, it is more difficult to copy the vein pattern and spoofing becomes much harder as compared to other biometric features.

In the scientific literature, usage of the hand vein pattern in biometrics started to be discussed in the early 1990s [4]. One of the first papers on this topic is published by Cross and Smith in 1995 [5]. They use dorsal (back of hand) vein pattern as a biometric feature. In this study, they propose using thermal imaging devices to capture dorsal hand vein images. However, as the thermal imaging technology is influenced by the ambient temperature, it is not widely be used in general applications.

Due to the dependence of hand vein images on practical data acquisition techniques, developments in imaging devices have increased the usability of hand vein patterns as a biometric feature. In the market, one of the first utilized patents is owned by Tech-Sphere Co., Ltd. in Korea in 1998 [6]. Meanwhile, different kinds of research groups and organizations have been working on development of new technologies on hand vein biometry. Thousands of biometric hand vein products have been rapidly installed and successfully used in various applications up to date [4]. These developments and high attention of biometric community on hand vein biometry shows us that it is one of the promising biometric technique in the security field.

2.1. Modeling The Architecture of A Hand Vein Recognition System

Similar to the other biometric systems, a typical hand vein recognition system consists of different modules including image acquisition, ROI determination, image processing, feature extraction and feature matching. Architecture of a hand vein recognition system is shown in Figure 2.1.

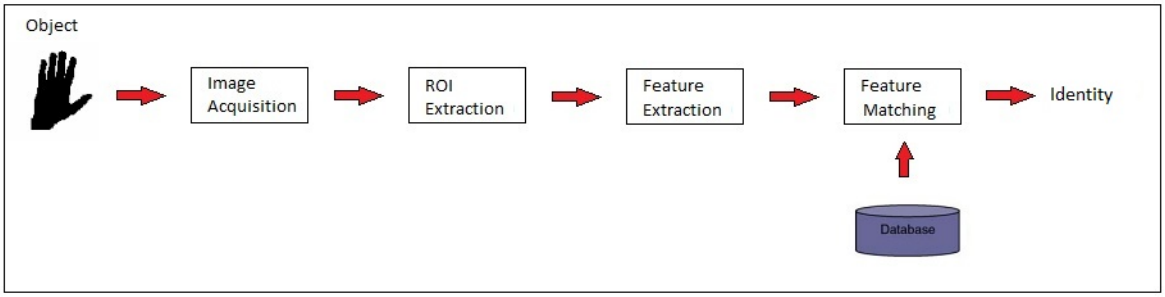

Figure 2.1. A typical architecture of a hand vein recognition system.

2.1.1. Image Acquisition

A hand vein network consists of two main vein systems namely palmar and dorsal metacarpal. Dorsal metacarpal veins spread into the back of the hand. There are mainly two types of veins on the dorsal metacarpal as cephalic and basilic. The basilic veins attach to the surface of the hand, whereas cephalic veins attach to the elbow of

the hand. Both basilic and cephalic veins are demonstrated and marked in Figure 2.2. Acquisition of qualified images is essential for a biometric system. For a dorsal hand

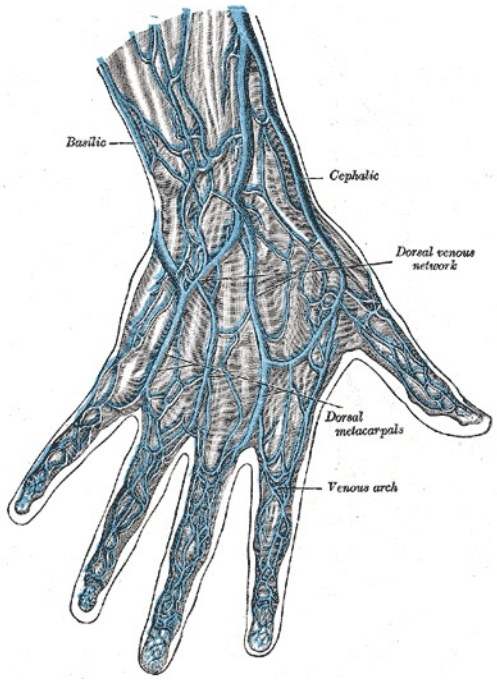

Figure 2.2. Dorsal venous network of the hand. Obtained from [7].

vein recognition system, a good quality of image is specified with retaining detailed biometric features in terms of cephalic and basilic veins. We have to know that any natural or disease based (diabetes, hypertension, atherosclerosis, metabolic disorders, tumors, etc.) deformations on the vein system and fatty, thick skin surface can change the quality of the captured images.

Image acquisition process of a dorsal vein biometric system could have differences on many aspects. The main factor is the image capturing devices. In addition to this, automatization of the acquisition, hand rotation and translation restrictions vary for each system.

2.1.1.1. Variations on Image Capturing Devices. Veins are found beneath the skin and generally they are not easily discernible in visible light. Because of the biological properties of the human tissues, the vein pattern can be observed in infrared light

(IR). In the electromagnetic spectrum, infrared refers to a special wavelength range of 0.75 to 1000 μm. This region is further divided into four sub-bands, namely near infrared (NIR) in the range of 0.75 μm to 2 μm, middle infrared (MIR) in the range of 2 μm to 6 μm, far infrared (FIR) in the range of 6 μm to 14 μm, and extreme infrared in the range of 14 μm to 1000 μm [7].

In the literature, image capturing stages which use MIR [8] and FIR light sources [7] can be referred as "thermal imaging". Thermal imaging method uses thermal cameras such as NEC Thermo Tracer and InfraCam and capture the emitted radiation from the body. Medical researchers have found that human veins have higher temperature than surrounding tissues and thus, thermal imaging can be used as a capturing method for vein images. One of the advantage of thermal imaging techniques is that they are not affected from the lighting conditions. Lin *et al.* [8] capture thermal images under random lighting conditions, even in a dark environment without any light source. Thermal imaging is also not affected from extra skin surface information such as hair. On the other hand, thermal images have many disadvantages on the quality of vein images. Firstly, they are influenced from ambient temperature and humidity strongly and they are very expensive. Wang *et al.* [7] capture thermal images in two environments; a normal office environment ($< 10\,^{\circ}\mathrm{C}$ and constant humidity) and a tropical outdoor environment ($30 - 34\,^{\circ}\mathrm{C}$ and > 80 per cent humidity) and observe that a tropical outside environment has negative impact on the thermal image quality. Examples of indoor and outdoor thermal images are given in Figure 2.3. Besides, in practise, most of the thermal images have low level contrast between veins and surrounding tissue which makes it difficult to separate the veins. Thermal images can capture only major vein pattern so it limits the image quality, as well. NIR imaging technique is the most commonly used image acquisition technique in dorsal hand vein biometric field [5], [7], [3], [1]. It utilizes the principle explained by photobiology . In biology, there is a "medical spectral window", which extends approximately from about 600 to 1100nm. The light in this window can penetrate deeply into tissues. Since NIR lighting is in this range, it can be used to see under skin. When a hand is exposed to NIR light, vein segments absorb the light more than the surrounding tissues and hence, they appear darker than the other hand partitions in a NIR image. There are

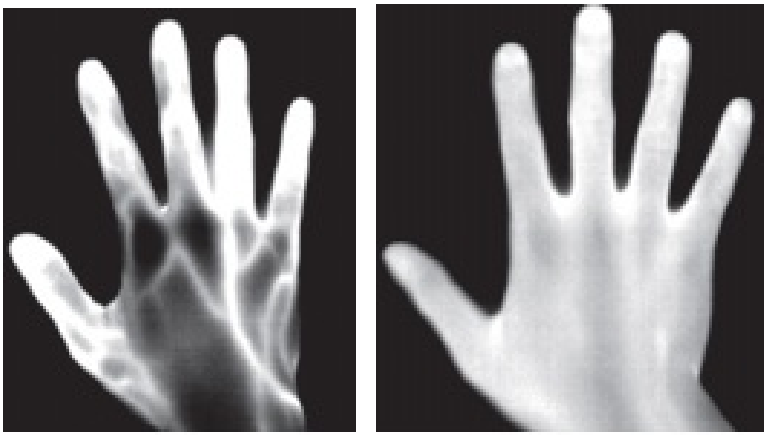

(a) (b)

Figure 2.3. Examples of (a) a thermal indoor image, (b) a thermal outdoor image.

two main NIR imaging issues that have to be known: First, as the depth of absorption and radiation of NIR in biological tissue is approximately $3mm$, only the subcutaneous vascular network is discernible in a NIR vein image. Secondly, using IR cold light source is the best lighting technique for NIR imaging since the reduced haemoglobin in venious blood absorbs more NIR light, and makes the veins much darker than the surrounding tissue. NIR imaging cameras have low cost but they are sensitive to the defects and hairs on the skin surface. Examples of capturing hair skin surface and no-hair skin surface is shown in Figure 2.4. Since it is also effected from environment lighting significantly, NIR imaging system needs an IR filter to eliminate other spectral light in the environment. Based on all these criteria, the best NIR imaging system could be constructed with a NIR sensitive charge-couple device (CCD) camera, an IR filter and an IR cold source such as NIR LEDs. In the dorsal hand vein literature, CCD cameras like JAI CV-M50 IR [9], and Hitachi KP-F2A [7] were used to capture images of veins found beneath the body surface. Near infrared LEDs with wavelength from $850nm$ [10] to $880nm$ [5] were used as the light source. To cutoff the visible light, IR filter with different cutoff wavelengths, λ, were devised. Some researches deployed IR filter with $\lambda \approx 800nm$ [7] and some used higher cutoff wavelengths at $900nm$ [5]. NIR images can be captured by either reflection or transmission methods. In the reflection method, hand is in front of the camera and the light source while it is between camera and the light source in the transmission method. Typical reflection and transmission

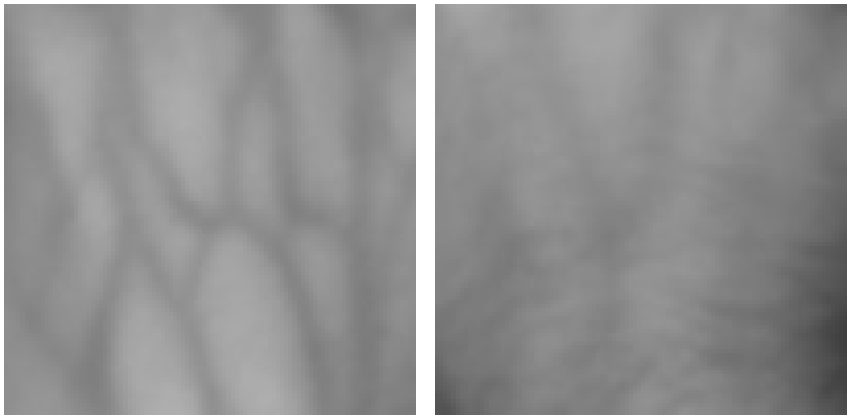

(a) (b)

Figure 2.4. Examples of NIR image of (a) the back of a hand, (b) the back of a hand with hair.

based system models are shown in Figure 2.5, respectively.

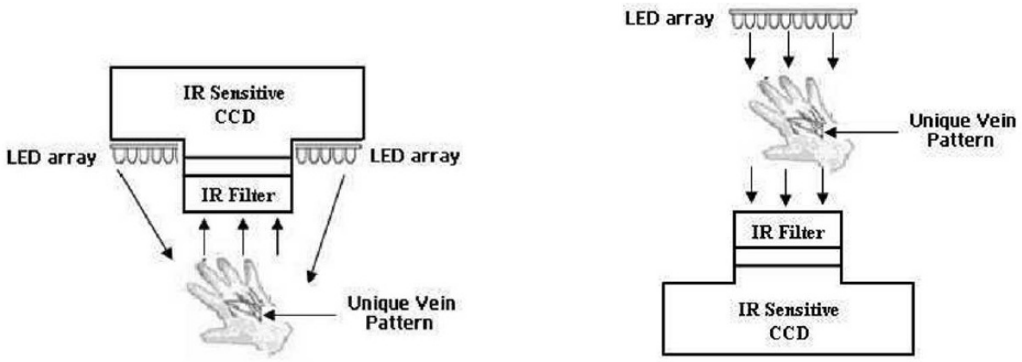

(a) (b)

Figure 2.5. Configuration of (a) reflection, (b) translation based hand vein image acquisition methods. Obtained from [4].

2.1.1.2. Other Variations. Apart from the image capturing device, an image acquisition system can vary on some other aspects. For example, the imaging setup in prior works [5], [11], [12] use a hand docking frame device, cavities for finger valleys or other form of restricted area to limit the translational and rotational changes which are often inconvenient and not user friendly. In Yuksel *et al.* [1], a free-form reflective NIR setup

has been used not to restrict the movement of the hand. Moreover, there is not any systematic, completely automated image setup for hand vein based recognition system, except for some works as Soni *et al.* [13] and [14], Besides, although they are not fully automated, Lin *et al.* [8] and Cross *et al.* [5] provide this criterion to some extent.

2.1.2. Region of Interest (ROI) Determination

ROI determination is very important since vein patterns should be extracted in the same region from all images to ensure the stability of the extracted vein features. There are several ways to stabilize the ROI. If an imaging setup guides the position of the hand by any restriction system, the captured images are at the same region, although some positional variations can be accepted. This has to be accounted on the feature matching stage, where a few shifting changes should be allowed.

Another way of ROI determination is to use information on the image after data capturing. In the literature, there are two types of captured images based on the hand posture. One is a relaxed hand position with all the fingers visible [1] as in Figure 2.6a. The other is a clenched fist where all the fingers are hidden [3] as in Figure 2.6b. In this type of ROI determination, one can select reference points according to the hand posture. If the hand has a relaxed position, reference points are selected as finger valleys and the wrist [8], [9], [1], or on the latter type, the outline of the hand or fingers is defined using hand object and background properties [5], [3], [15], [13]. According to these reference points, the image is rotated until these references are on standard positions. Sometimes, size normalization is also done in this stage.

Several methods use both two ROI determination techniques and in addition to this, allow for adaptations in the feature matching process.

2.1.3. Image Preprocessing

Although image preprocessing stage is an optional process, it is widely used to enhance the quality of images. The acquired image contains information that is irrel-

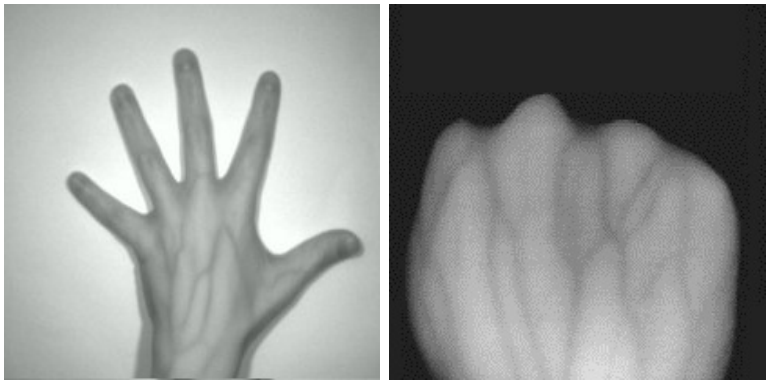

(a) (b)

Figure 2.6. Examples of (a) a relaxed, (b) a clenched fist hand position in a hand vein image.

evant for recognition, such as background noise, irregular shades because of the bones and muscles in the finger and intensity fluctuations. The aim of image processing is to enhance the desired vein pattern and get rid off irrelevant information.

Image processing is mainly done with filtering operations. In some methods, processing consists of several consecutive filters and algorithms. In the literature, for noise reduction and smoothing Mean filtering [13], Median filtering [8], [3], Non-Linear Diffusion filtering [3], 2D Wiener filtering [9], [15], Gaussian Low Pass filtering [7], [13] and Matched filtering [15] are widely used.

If a biometric system does not use preprocessing and normalization techniques, the feature extraction modules should be more robust against images with noise and illumination changes.

2.1.4. Feature Extraction

Dorsal hand vein recognition methods can be categorized into two types as appearance-based and geometry based approaches. Appearance based approaches may use subspace-based features which allows effective characterization of a low-dimensional subspace within the raw image's overall space. For hand vein recognition, the process

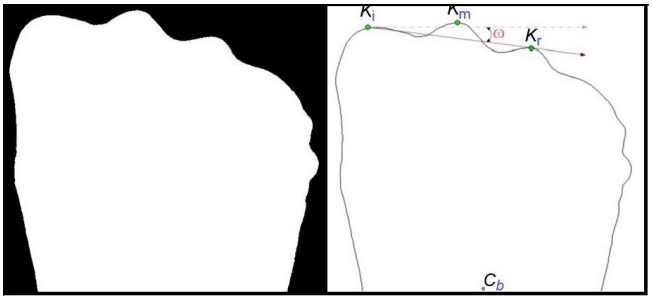

(a)

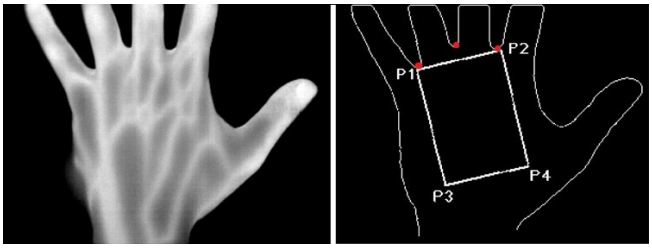

(b)

Figure 2.7. ROI determination based on finding (a) knuckle tips, (b) finger valleys as key points.

firstly obtains a low-dimensional representation of the hand, then standard statistical methods are used to learn the range of appearance that the target exhibits in the new, low dimensional space. The advantages of subspace-based features is that they are generative and simple to characterize. Furthermore, they serve to reconstruct a hand image from its subspace with ignorable error. In the literature, Principal Component Analysis (PCA) [16], [17], Linear Discriminant Analysis (LDA) [18], [17], Independent Component Analysis (ICA) [1], Non-negative Matrix Factorization (NMF) [1] and their kernelized versions are used to extract dorsal hand vein patterns from images.

Geometry based approaches extract vein based features on the base of the locations and local statistics such as line segments, minutiae points and ridge bifurcations (knuckle, joint) of the vein pattern. The goal in these methods is representing skeleton or medial axis of the vein structure. Although edge and ridge detectors are used to extract these features [8], [9], they are not suitable to extract these features. The common method on segmentation of the vein pattern consists of thresholding and skeletonization steps [19], [1]. Since the intensity values of the vein vary across the image,

local adaptive thresholding techniques give more satisfactory results than global ones. Yuksel et. al. [1] compares several thresholding methods on hand vein images which are Yasuda [20], Bernsen [20], Niblack [20], Wang [7] local thresholding and Otsu [20] global thresholding method. According to this work, the best results for hand vein biometry are obtained with the Yasuda method. For computing skeletons, there are many different algorithms for shapes in digital images, such as using morphological operators, supplementing morphological operators with shape based pruning, using curve evolution, using level sets, finding ridge points on the distance function, "peeling" the shape, without changing the topology, until convergence. Based on the required feature, additional approaches can be applied on skeletonized vein image. For example, to extract minutiae and knuckle points of the vein structure, polynomial curve fitting is applied on the images [9]. Moreover, to construct a graph form from vein structure description, line segmentation algorithms could also be used [1], [7].

Local features which are tailored to hand images could be other interesting classes of features. Some of the examples are Gabor wavelets, local binary patterns (LBP) [15], Scale Invariant Feature Transform (SIFT) feature descriptors [21], [22] and gradient field. They become capable of representing both local properties and their configurational information when these features are treated along their spatial coordinates.

According to Cross *et al.* [5] while segmenting vein patterns from the background generally five types of segmentation errors are encountered:

- Mismeasured attributes: Noise can cause quantitative measurement errors in the segmented image. For example, the length of a vein of a unique hand might appear longer or smaller in different images.
- Missing objects: If an object is not clearly visible due to glance, shadows or occlusion it will not be represented in the segmented image.
- False objects: Large marks or shadows appear as feature objects in the segmented image.
- Fragmented objects (over segmentation): noise can cause fake edges and fragment one object into several regions in the segmented image.

- Merged objects (under segmentation): Noise can cause blurred edges, resulting in two or more objects merged together as one region in the segmented image.

Because vein images usually contain a lot of noise due to the complex structure of the tissue, bones and skin surface, feature extraction methods should be robust enough to overcome errors. In addition, the quality of the images after image processing should be as high as possible, but not excessively manipulated.

2.1.4.1. Feature Matching. In this stage, the features of a template image already stored in the database are compared to the test image. According to the purpose of the system (identification or verification), this can be done as a one-to-one match or a one-to-many database search.

For hand-vein biometric setup, feature matching of ROI images with simple pixel by pixel comparison is not suitable due to the following reasons:

(i) Since ROI images contain extra information such as skin, hair, and spiloma, using ROI images will cause interference of these with vein patterns.
(ii) The subcutaneous blood vessels can move with some freedom according to the shape of the hand which influences the stretching of veins.
(iii) The diameters of the veins may vary as a result of weather circumstances and physical activities.

Due to above factors, a hand-vein biometric system requires features to be extracted based on vein patterns and tries to match the identities by using them. Depending on the types of features extracted, different matching methods were used to compare template and test identities. Based on the used features, these techniques could be decomposed into two categories: geometry based matching, and appearance based matching. The geometry based matching techniques compare the geometrical features like line segments, minutiae points and ridge bifurcations (knuckle, joint) of the vein pattern. If a vein pattern is defined by line based features, Euclidean distance

could be applied on computing the similarity or dissimilarity, between two line segments which are represented in the Z^2 coordinate system. Line based matching on the whole is more informative rather than point-based matching since a vein pattern could be better characterized using the rich line features as compared to minutiae or joint points. Feature-based matching works well for appearance-based approaches. For research which studied the subspace-based methods like PCA, LDA, ICA and NMF, adopted Euclidean distances or cosine similarity are chosen by the most of the authors to compute the matching scores. For the other studies, a variety of distance metrics like Euclidean distance, city-block distance, and chi square distances were used. When low-resolution images are used for hand vein biometry, feature based matching has a great advantage over geometry based matching. This is due to the fact that geometry-based matching mostly needs higher resolution images to acquire precise location and orientation of the geometrical features.

2.2. Comparative Summary of Prior Works

In order to compare the prior works on hand vein biometric field, we report each system on the basis of six criteria; namely, image capture, database, ROI determination, image preprocessing, feature extraction, feature matching and performance. Table 2.1 represents each work with above criteria, schematically.

Table 2.1. Comparative summary of prior works on dorsal hand vein biometric field.

Reference	Image Capturing	Database	ROI Determination	Image Processing	Feature Extraction	Feature Matching	Performance
Lin et al. [8]	MIR Thermal Camera	32 subjects, 30 samples/subjects, total 960 images	Binarization, distance center wrist to borders, use 2nd and 4th finger valleys to obtain ROI	Median filtering	Watershed transformation, feature points, feature point image	Moment, mean and counter filter: multi resolution of FPs, PBF integration, verification threshold	FAR - 1.5 % FRR - 3.5 %
Badawi [3]	NIR CCD camera, IR filter, IR cold source, docking frame	500 subjects, 10 samples/subjects, total 5000 images	Binarization, center hand segment	Smoothing, noise reduction: Median filtering, non-linear diffusion filtering	Binary image after average thresholding	The ratio of the count of overlapped white pixels	FAR - 0.03 % FRR - 7.84 %
Khan et al. [16]	-	Badawi's DB is used\cite{Badawi2006}	-	Median filtering, Background subtraction, vein thresholding, thinning	Quadratic Inference Function (QIF)	Euclidean Distance	FAR - 0.020 % FRR - 0.030 %
Wang et al. [9]	FIR thermal camera, hand position restriction	47 subjects, total 141 images	Sobel filter, distance center wrist to borders, use 2nd and 4th finger valleys to obtain square	Noise reduction: Median filtering, 2D-Wiener filtering	Normalization, local thresholding with global reduction, skeletonization, polynomial curve fitting, minutiae feature extraction	Modified Hausdorff Distance	EER - 0 %
Wang et al. [19]	Setup #1: FIR thermal camera, position restriction, Setup #2: NIR CCD camera, IR filter, IR cold source, position restriction	Setup #1: 30 subjects, 270 images Setup #2: 150 subjects, 3 (back of hand), 3 (palm),3 (wrist) samples/subjects, total 2700 images	Sobel filter, distance center wrist to borders, use 2nd and 4th finger valleys to obtain square	Noise reduction: Median filtering, Gaussian Low Pass filtering	Normalization, local thresholding, skeletonization, smoothing	Line segment Hausdorff Distance (LHD)	Setup #1: FAR - 0 % FRR - 0 % EER - 0 % Setup #2: better than Setup #1
Cross et al. [5]	NIR CCD camera, IR filter, IR cold source, docking frame	20 subjects, 5 samples/subjects	Morphological gradient separation fore/background, erosion	Noise reduction and contrast enhancement: moving average	Brightness subtraction, morphological thresholding & Thinning and pruning algorithm: medial vein axis representation	Superimpose and correlation: forward and reverse similarity of dilated test/reference image	FAR - 0 % FRR - 7.5 %
Wang et al. [15]	a low cost NIR camera, hand position restriction	102 subjects, 20 samples/subjects, total 2040 images	use centroid to obtain square, noise reduction: Matched, Wiener and smoothing filtering	gray scale normalization, segmentation by Zhao et al.\cite{Zhao2007}' image segment method	Partition Local Binary Pattern (PLBP)	Chi square statistic similarity measurement	IR - 90.88 %
Zhao et al. [19]	low cost NIR camera, IR filter, IR cold source	NO INFO	NO INFO	Noise reduction: Matched filtering, Wiener filtering, smoothing filtering	An improved local dynamic threshold segment method, morphological processing, thinning and pruning	-	-
Soni et al. [13]	automatic system; simple digital SLR camera, IR filter, a low cost night vision lamp	341 subjects, total 1750 images	Sobel filter, distance center wrist to borders, use 2nd and 4th finger valleys to obtain square	Segmentation with active contouring, skin component of the image is ROI	Grey scale conversion, Gaussian filtering, Mean filtering, Connected Component Labeling (CCL)	A Euclidean based matching technique	Accuracy - 99.26 % FRR - 0.03 %

3. GEOMETRY BASED HAND VEIN BIOMETRY

3.1. Outline of the System

In this thesis, we construct a dorsal hand vein recognition system based on geometry based hand vein processing. Our hand vein biometry system consists of three main steps which are normalization of the hand position and ROI extraction, geometry based feature extraction and pattern matching. Figure 3.1 shows the outline of the system. In our system, we work on the publicly available Bosphorus Hand Vein Image

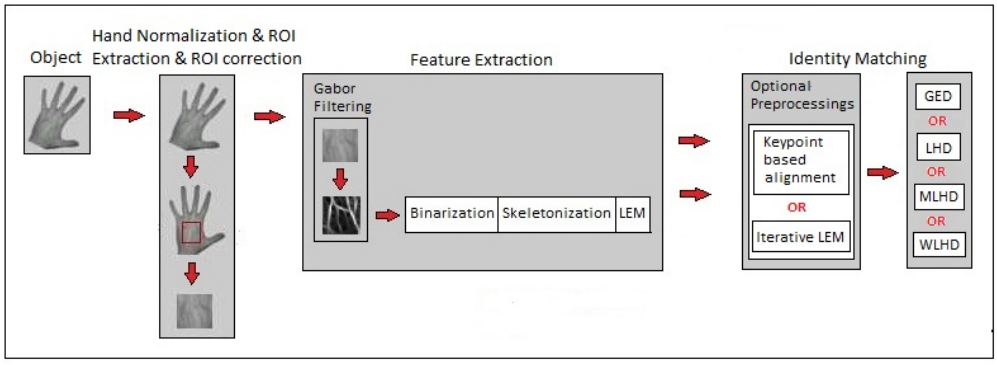

Figure 3.1. The steps of our dorsal hand vein biometry system.

Database [1]. The hand vein images are consecutively processed by these processes: Firstly, ROI images are extracted from the raw images and a Gabor filtering based vein enhancement technique is applied to them. For the vein feature extraction, we prefer geometry based features as vein line segments and junction points. These line segments are then converted into a graph form, and line segment and graph similarity measures are used for matching.

3.2. Hand Normalization and ROI Extraction

3.2.1. Yoruk Algorithm

For all biometric systems, data which has been reliably registered increases the success rate. Therefore, hand normalization and ROI extraction are of capital importance for a hand vein biometric system.

The Bosphorus Hand Vein Image Database consists of hand vein images of hands with arbitrary positions but all fingers are separated and visible. Since the capturing setup does not have a docking hand device, the key points such as the finger tips and finger valleys are not marked in acquisition. Accordingly, we need a method to normalize the hand position, to find the key points and then extract ROI. For this purpose, we use Yoruk's algorithm [23], [24].

Yoruk algorithm is designed for shape-based hand recognition. It re-positions hand images to a fixed pose by not only rotating and translating hand but also normalizing positions of individual fingers. Yoruk algorithm consists of mainly six processing stages, namely segmentation of the hand image from the background, hand rotation and translation, finding the finger axes and tips, completion of the wrist, rotation and translation of fingers to standard orientations around estimated finger pivots:

- Hand segmentation: First, Yoruk algorithm extracts the hand from the background. It uses the 2-means clustering algorithm which is followed by morphological operators to fill in holes and remove isolated foreground debris. After that, it applies a "ring artifact removal algorithm" to get rid of any straights that the rings can cause. A binary image, corresponding to the silhouette of the hand, is extracted as the outcome of this stage.
- Initial hand registration: This step involves translation and rotation operations. The outcome of the hand segmentation stage, binary hand image is translated according to the centroid of the binary hand mass and rotated in the direction of the larger eigenvector of the inertia matrix. Inertia matrix can be envisioned as

an ellipse fit to the hand object, where the larger eigenvalue determines the hand orientation and corresponds to the major axis of that ellipse.

- Finding finger tips and valleys: The finger tips and the finger valleys are extracted by computing the radial distances with respect to a reference point around the wrist region. This reference point was taken as the first intersection point of the major axis with the wrist line. The resulting sequence of radial distances yields 4 minima and 5 maxima points corresponding to finger tips and valleys, respectively.
- Wrist completion: The wrist contour can be ambiguous due to some noisy effects of occlusion, the different wrist postures or imaging device. In order to create similar wrist contour for every hand image, wrist region is tapered off from the half distance between the pivot line and the wrist line.
- Finger pivots: A hand has an ability to locate the fingers on different orientations. Thus, in order to normalize the hand, there is a also need for the rotate and translate the fingers separately. Fingers are aligned by being reoriented along predetermined directions around their finger pivots.

In this thesis, we do not need the exact translation and rotation of fingers, our requirement is normalization of back of the palm area. Besides, Yoruk algorithm's wrist completion module removes the vein information around the wrist and this causes loss of information. Because of these, we utilize the first three stages of Yoruk algorithm, which are hand segmentation, initial hand registration and finding finger tips and valleys. After determination of finger tips and valleys, we select dorsal hand ROI as a rectangle, the two corners of which are the valley between small finger and ring finger, and the valley between the middle finger and index finger. In our case, the outcome of hand normalization and ROI extraction stage is the 100x100 ROI image patch which is extracted from the normalized palm.

3.2.2. Warping Hand Segments by Thin Plate Spline

Investigation of hand vein images shows us that, two hand segments of a person can differ according to the pose of the captured hand. Vein orientations and the spatial

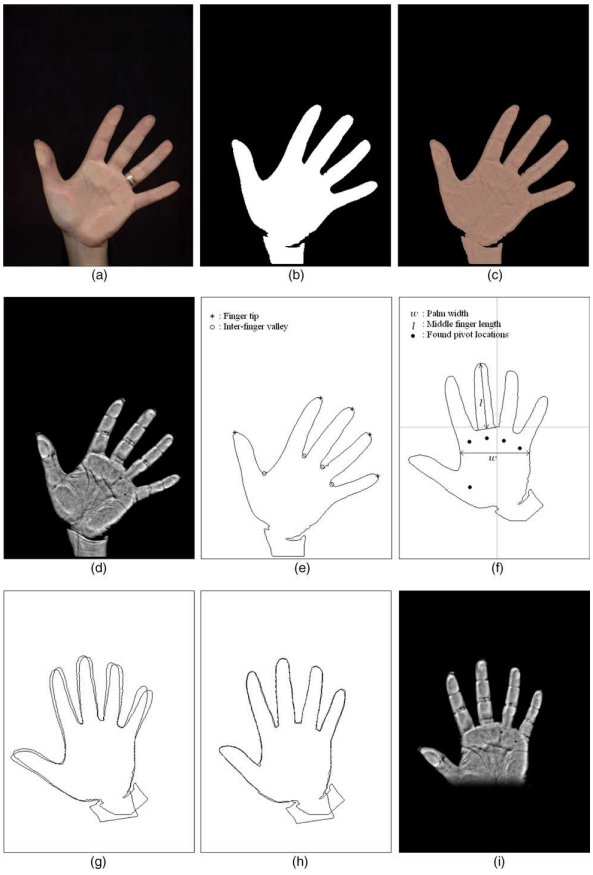

Figure 3.2. Processing steps for hand normalization obtained from [24]: (a) original hand, (b) segmented hand, (c) illumination corrected hand, (d) texture enhanced hand, (e) determination of finger tips and valleys, (f) initial global registration by translation and rotation, (g) superposed contours of the same individual, (h) superposed contours of the same individual, (i) final normalized hand.

difference in between two vein segments result in this alteration. To illustrate this, Figure 3.3 is given. These ROIs belong to the same person. Though ROI (a) and ROI (b) contain the same vein segments, they appear to be closer at the bottom right side of the ROI (b). To decrease this effect, we aim to warp all hand vein segments before extracting ROIs to a model hand segment template for aligning the same vein segments to the same spatial position. We use Thin Plate Spline (TPS) warping method for this purpose.

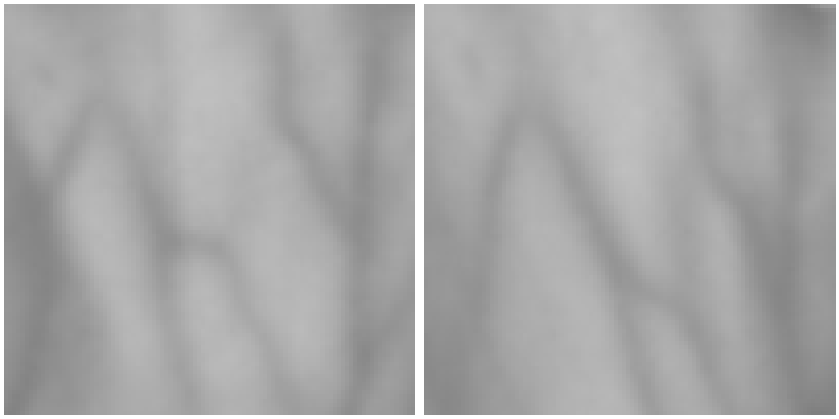

(a) (b)

Figure 3.3. Two ROIs belong to the same person.

3.2.2.1. Thin Plate Spline (TPS). TPS is an algebraic approach which expresses the dependence of the physical bending energy of a thin metal plate on point constraints [25]. For two templates in which the corresponding landmarks are given, TPS warping deforms the first template to the other one by transforming corresponding landmarks exactly. The key point of this transformation is minimizing the total bending energy at all points of the transformed template.

The hand vein image is modeled by:

$$z(x, y) = -U(r) = -r^2 log r^2 \tag{3.1}$$

$z = (x, y)$ is the thin plate surface function where r is defined as the distance of point

(x, y) to the Cartesian origin.

The bending energy at a point of a thin plate surface is defined as:

$$E(x,y) = (\frac{\partial^2 z}{\partial x^2})^2 + 2(\frac{\partial^2 z}{\partial x \partial y})^2 + (\frac{\partial^2 z}{\partial y^2})^2 \tag{3.2}$$

In order to minimize the total bending energy of a thin plate surface, the bending energies at all points in a surface has to be considered. This minimization equation, named as the *integral bending norm*, is given below:

$$\int_R \int (\frac{\partial^2 z}{\partial x^2})^2 + 2(\frac{\partial^2 z}{\partial x \partial y})^2 + (\frac{\partial^2 z}{\partial y^2})^2 dxdy \tag{3.3}$$

Suppose that we have two point sets $P_i = (x_i, y_i), i = 1, ..., n$ and $P_i' = (x_i, y_i), i = 1, ..., n$ which are given as landmark points for two templates. Function $f(x, y) = [f_x(x, y), f_y(x, y)]$ maps point set P_i to P_i' as much as possible by preserving *integral bending norm*.

The *integral bending norm* equation can be converted into the weighted sums of basis U functions. The following derivations demonstrates how to obtain these weighted sum values.

Let $r_{ij} = |P_i - P_j|$ is the Euclidean distance between P_i and P_j. The rest equations are:

$$K = \begin{bmatrix} 0 & U(r_{12}) & \cdots & U(r_{1n}) \\ U(r_{21}) & 0 & \cdots & U(r_{2n}) \\ \vdots & \ddots & \ddots & \vdots \\ U(r_{n1}) & U(r_{n2}) & \cdots & 0 \end{bmatrix} \tag{3.4}$$

$$P = \begin{bmatrix} 1 & x_1 & y_1 \\ 1 & x_2 & y_2 \\ \ddots & \ddots & \ddots \\ 1 & x_n & y_n \end{bmatrix} \tag{3.5}$$

and

$$L = \left[\begin{array}{c|c} K & P \\ \hline P^T & O \end{array}\right] \tag{3.6}$$

where O is a 3x3 zero matrix. Let V is an nx2 matrix consists of homologous of P_i landmark points:

$$V = \begin{bmatrix} x'_1 & x'_2 & \ddots & x'_n \\ y'_1 & y'_2 & \ddots & y'_n \end{bmatrix} \tag{3.7}$$

Depending on L and V matrix $W = (w_1, w_2, ..., w_n)$, a_1, a_x and a_y are defined as:

$$L(V|0,0,0)^T = (W|a_1, a_x, a_y)^T \tag{3.8}$$

The function f(x,y) is derived as:

$$f(x,y) = a_1 + a_x x + a_y y + \sum_{i=1}^{n} w_i U(P_i - (x,y)) \tag{3.9}$$

Since f(x,y) minimizes the nonnegative quantity over all class of interpolants, it preserves *integral bending norm* I_f as:

$$I_f = \int_R \int (\frac{\partial^2 f}{\partial x^2})^2 + 2(\frac{\partial^2 f}{\partial x \partial y})^2 + (\frac{\partial^2 f}{\partial y^2})^2 dxdy \tag{3.10}$$

3.2.2.2. Applying TPS to hand vein ROIs. In order to apply TPS method to two given templates, corresponding reference points of these templates have to be known.

As mentioned in Section 3.2.1, Yoruk algorithm finds normalization angle and finger valleys for each hand segment while extracting ROI. Since these valleys represent homologous points for each hand vein segment, we accept them as TPS reference points. Figure 3.4 shows these valleys in a hand segment.

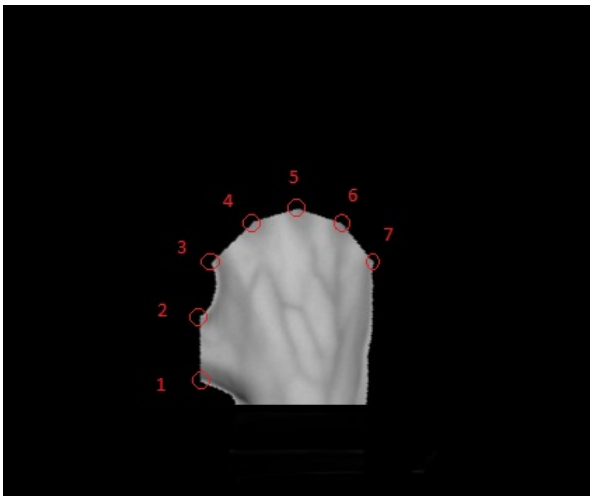

Figure 3.4. Finger valleys of a hand. Thumb stands between first and second valleys where index finger is between third and fourth ones. The rest middle, ring and little fingers locate between fourth and fifth, fifth and sixth, sixth and seventh valleys, respectively.

Let seven valleys for each hand vein segment represent $P_i = (x_i, y_i), i = 1, ..., 7$. To map P_i to P'_i, we need a reference P'_i set of a reference hand. Rather than selecting a reference hand, we utilize 100 truly normalized hand vein segments from 50 different subjects. By calculating mean finger valleys of these segments, reference finger valleys are constructed and accepted as P'_i. Each hand vein segment in the database is warped on the base of P'_i and then ROIs are extracted. The difference between non-warped and warped hand segments' ROIs is demonstrated in Figure 3.5.

However, warping is not successful if the finger pivots are not extracted successfully. The effects of warping on the success rate does not give expected results. These results and their possible reasons are given in Chapter 4. Since non-warped hand segments provide more promising results than warped hand segments, we prefer to use

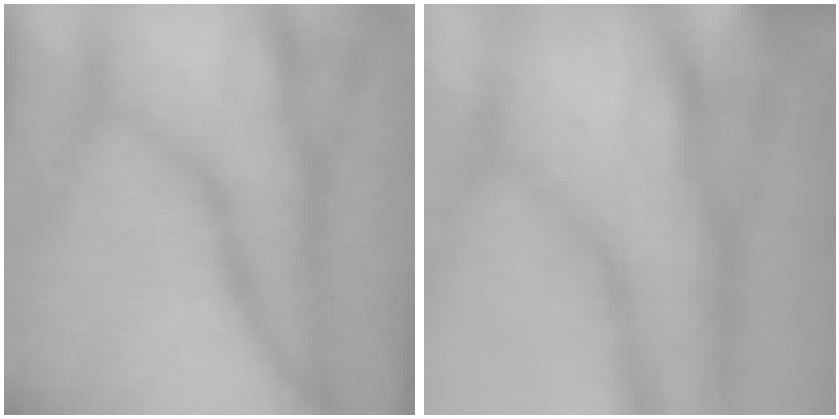

(a) (b)

Figure 3.5. Two ROIs belong to the same person: (a) Hand segment is not warped, (b) Hand segment is warped before ROI extraction.

non-warped hand segments for further processes.

3.2.3. Enhancing ROIs by mean intensity value

Finding the correct location of the finger tips and valleys can be impossible if the hand vein image is influenced by extreme illumination effects. For example, if the fingers are so close to each other, the visibility of the finger valleys deteriorates or if the subject wears any accessories in the near of wrist (brace, watch, etc.), wrist line can be detected erroneously. We notice that the wrong detections are mostly caused by finger valleys rather than wrist accessories. To illustrate this, the examples of correctly and wrongly extracted ROIs are shown in Figure 3.6. We propose a ROI enhancement method to crop the extraneous information from extracted ROIs. Firstly, we inspect the ROIs and decompose them into two groups as correctly and incorrectly extracted. As the result of the data inspection, we notice that the irrelevant information appears darker in a ROI image, hence it decreases the image's mean intensity value. The wrong ROIs' mean intensities are smaller than a threshold ($T = 50$) where each ROI's pixel intensity is in the range of 0 and 255. However, some correctly extracted ROIs can also have lower intensity than the threshold value since hair, spiloma or hand bones can diminish the mean intensity. According to these issues, we construct an enhancement

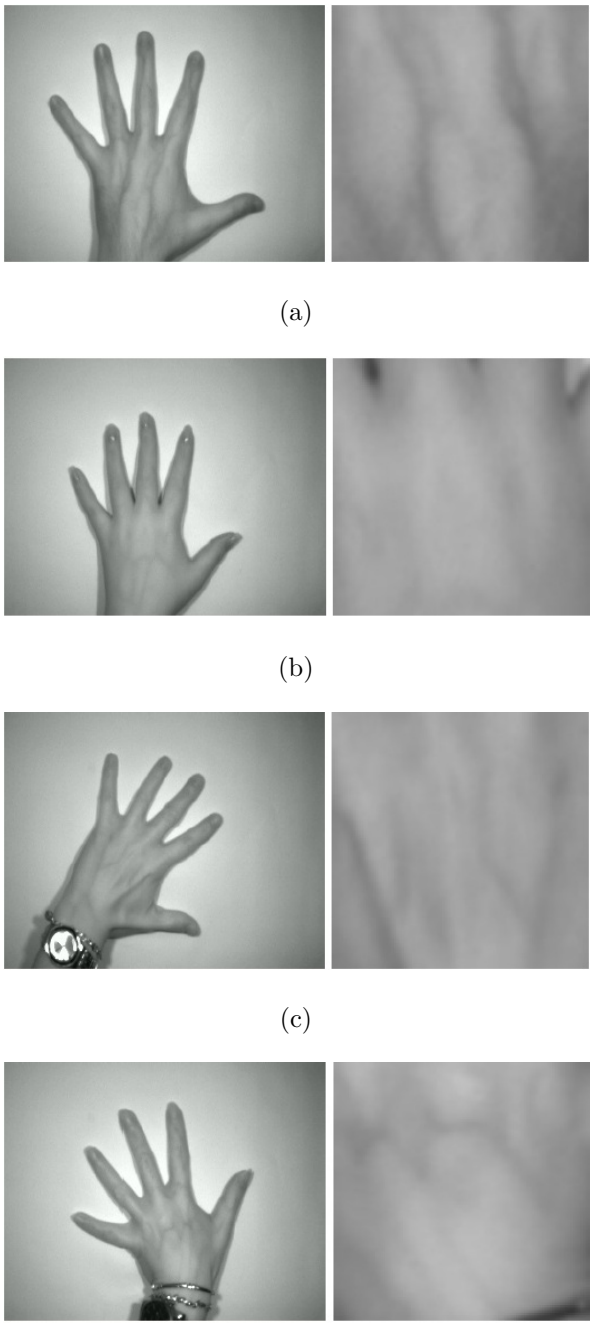

(a)

(b)

(c)

(d)

Figure 3.6. Examples of ROIs. First columns are the raw images whereas the second columns on the same row are their corresponding ROIs; (a) a correctly extracted ROI, (b) a wrongly extracted ROI which includes irrelevant information at the finger field, (c) a correctly extracted ROI tolerant to wrist accessories, (d) a wrongly extracted ROI which has irrelevant information around wrist.

method based on the mean intensity values of ROI images. The flowchart of this enhancement method is given in Figure 3.7.

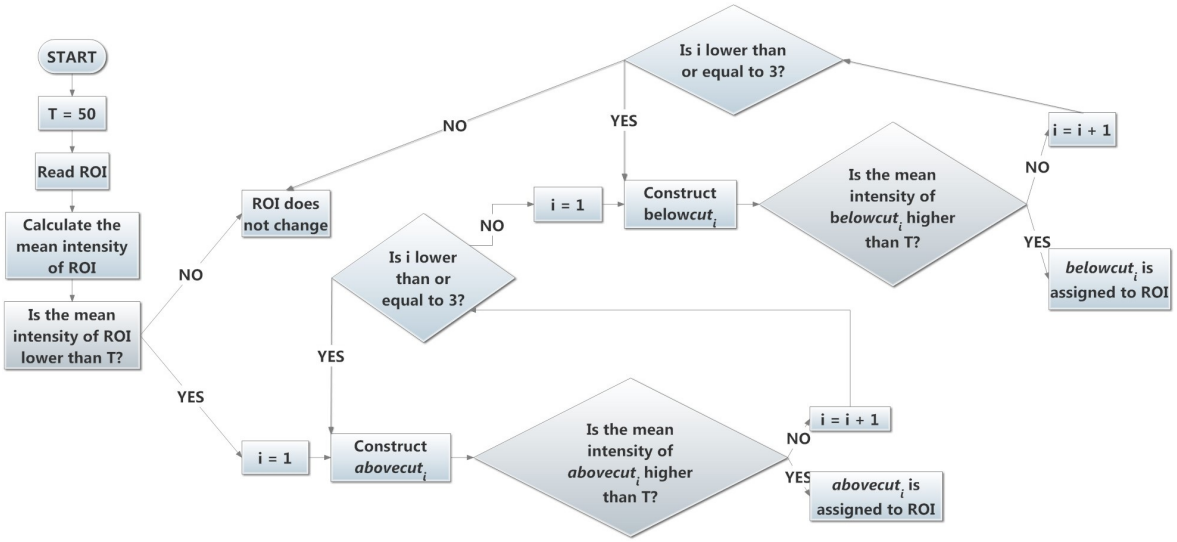

Figure 3.7. The flowchart of ROI enhancement method.

According to the data inspection, we notice that irrelevant information on the incorrectly extracted ROIs are located in the approximately above or below fifteen rows. Since the irrelevant information is more likely located above the image rather than below, we start to cut the ROI from above iteratively. Suppose that $abovecut_i$ shows the above cut image in the ith iteration. In each iteration, we cut $i * 5$ rows from the above. If the $abovecut_i$'s mean value is higher than the threshold, $abovecut_i$ is selected as ROI and the process is stopped. If at the end of the third iteration $abovecut_i$ is not selected as ROI, the process starts to investigate the image from below. Suppose that $belowcut_i$ shows the below cut image in the ith iteration. The same operations are repeated for $belowcut_i$. If at the end of the third iteration $belowcut_i$ is not selected as ROI, the process stops and ROI does not change. It means that, the mean intensity of the image is not affected from any irrelevant information, it is possible that the hand has some physical properties as hair, spiloma or obvious hand bones.

3.3. Feature Extraction via a Geometry based Method

Generally, a hand vein biometry system extracts features by appearance-based or geometry-based methods. In this thesis, we use a geometry-based method in which the veins are skeletonized by thinning and a graph is described through these thinned vein lines.

In most of the recent geometry-based feature extracting methods, ROI images are smoothed before skeletonization in order to alleviate the effects of noise. However, they do not improve the visibility of veins on hand image. In order to enhance the vein segmentation, we use two different even-symmetric Gabor filters banks to improve vein visibility and extract vein network more reliably. One of these banks is Yang. *et al.*'s [26] even symmetric Gabor filters bank and the other one is our proposed Gabor filters bank.

Both of the Gabor filters banks yield enhanced grey level hand vein images. In order to define geometric representation of hand veins, we first binarize the enhanced images by Yasuda thresholding method into two classes as vein segments (white) and the background (black). After that, vein segments are skeletonized by thinning to extract line segments from these images and converted to a graph structure by Line Edge Map (LEM) algorithm. As the outcome of feature extraction process, each hand vein structure is represented as a graph form.

3.3.1. Gabor Filtering

Gabor filters were modelled after the discovery of human visual cortex. Daugman [27], [28] developed a generalized Gabor function model that describes the receptive fields of the orientation-selective simple cells in the visual cortex. These were generalized to 2D Gabor filters and used extensively in various computer vision applications.

A Gabor function is obtained by modulating a sinusoid with a Gaussian. For one dimensional (1D) signals, a 1D sinusoid is modulated with a Gaussian; whereas, for 2D

signals such as an image, a 2D sinusoid is modulated. Subtracting DC response, a 2D Gabor filters can be declared as a function composed by a Gaussian-shaped function and a complex plane wave. Daugman and Lee *et al.* defined it as [28], [29]:

$$G(x,y) = \frac{\gamma}{2\pi\sigma^2}\exp\{-\frac{1}{2}(\frac{x_\theta + \gamma^2 y_\theta^2}{\sigma^2})\} \times (\exp(\hat{\jmath}2\pi f_0 x_\theta) - \exp(-\frac{\upsilon^2}{2})) \tag{3.11}$$

where $\hat{\jmath} = \sqrt{-1}$, θ describes the orientation of a Gabor filters, f_θ is the filter center frequency, σ denotes the standard deviation (often called scale), γ and υ represent the aspect ratio of the elliptical Gaussian envelope and the factor determining DC response, respectively. Moreover, $x_\theta = (xcos\theta + ysin\theta)$ and $x_\theta = (-xsin\theta + ycos\theta)$ are rotated versions of the x and y coordinates.

Gabor filters' response is widely used in vision based biometric systems such as iris, fingerprint, palm print recognition since it effectively represents local image information. In hand vein biometry, Gabor wavelets are used as local features tailored to hand images. For example, Lin *et al.* [8] extracted mean Gabor magnitude features from hand vein images classify the identities on the base of Gabor features.

Since hand veins vary in diameter and orientation, there is a need for a vein enhancement method which works reliably on different vein orientations and scales. Gabor filters can be sensitized to specific orientation and scale by selecting proper parameters. Constructing a Gabor filters bank from dissimilar Gabor functions can solve this problem.

3.3.2. Even-symmetric Gabor Filters

A Gabor filters can be decomposed into a real and an imaginary part using the Euler formula. The real part usually called even-symmetric Gabor filters, is beneficial to ridge detection whereas the imaginary part usually called as odd-symmetric Gabor filters, is suitable for edge detection. Since veins are seen as dark ridges in a hand image, a bank of even-symmetric Gabor filters can properly be used for hand vein

detection. An even-symmetric Gabor filters is defined as:

$$G^e(x,y) = \frac{\gamma}{2\pi\sigma^2}\exp\{-\frac{1}{2}(\frac{x_\theta + \gamma^2 y_\theta^2}{\sigma^2})\} \times (cos(2\pi f_0 x_\theta) - \exp(-\frac{\upsilon^2}{2})) \tag{3.12}$$

Yang *et al.* [26] used oriented Gabor filters on finger vein images to explore underlying finger vein information and reconstruct an enhanced finger-vein image. They constructed a bank of even-symmetric Gabor filters and generated differently transformed versions of an image using 2D convolution operation. However, to the best of our knowledge, no public hand vein biometric verification system is supplied presently which uses Gabor filters for enhancing vein segments in a hand image.

The processes of this enhancement method could be decomposed into two main partitions as Gabor filters bank construction and parameter selection, and enhanced hand vein image construction. In this thesis, we used Yang *et al.* [26] Gabor filters bank by modifying its image reconstruction procedure. Furthermore, we also construct another Gabor filters bank and use it for image enhancement.

3.3.2.1. Even-symmetric Gabor filters bank construction and parameter selection. We know that a hand vein network consists of vein segments in different size and orientations. The idea behind the even-symmetric Gabor filters bank is constructing a Gabor filters set and extracting each vein segment as the response of the corresponding Gabor filters. A filter in the even-symmetric Gabor filters bank is described as [26]:

$$G^e_{mk}(x,y) = \frac{\gamma}{2\pi\sigma^2}\exp\{-\frac{1}{2}(\frac{x_\theta + \gamma^2 y_\theta^2}{\sigma^2})\} \times (cos(2\pi f_0 x_\theta) - \exp(-\frac{\upsilon^2}{2})) \tag{3.13}$$

where m is the scale index and k is the orientation index and $\upsilon = \sqrt{2ln2/\beta}$ is satisfying for DC response subtraction [29] (β is defined in Equation 3.16). This filter bank subtracts DC response in order not to respond to the absolute intensity of the images.

We have also developed another even-symmetric Gabor filters bank and compared the effectiveness of both banks. Our proposed bank consists of even-symmetric Gabor

Filters represented as:

$$G^{e}_{mk}(x,y) = \exp\{-\frac{1}{2}(\frac{x_\theta + \gamma^2 y_\theta^2}{\sigma^2})\} \times (cos(2\pi f_0 x_\theta)) \tag{3.14}$$

where m is the scale index and k is the orientation index, either.

The Gaussian-shaped function of a Gabor filters is known as the Gaussian envelope. The Gaussian envelope and its parameters in the half-magnitude elliptic profile in frequency domain can be seen in Figure 3.8. According to Movellan [30], to facilitate

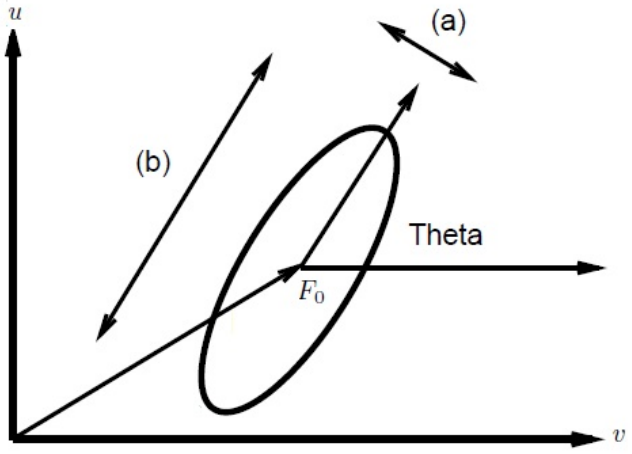

Figure 3.8. Parameters of the Gabor kernel as reflected in the half-magnitude elliptic profile in frequency domain.

the Gabor filters bank design, the half-magnitude contour of a frequency band should coincide with the lower contour of the next frequency band. To obtain the enveloped depicting the half-magnitude of filter responses between two adjacent scales in the frequency domain as shown in Figure 3.8, the following relationships should be observed [29], [31], [30]:

$$\begin{cases} \sigma_m = \sqrt{ln2/2}/(f_m \beta \pi) \\ f_m = R f_{m-1} \\ \Delta\phi \approx 2arcsin(a_m/2f_m) \end{cases} \tag{3.15}$$

where

$$\begin{cases} \beta = (2^{\Delta\omega} - 1)/(2^{\Delta\omega} + 1) \\ R = (1 + \beta)/(1 - \beta) \\ \Delta\phi \approx 2arcsin(a_m/2f_m) \end{cases} \tag{3.16}$$

a_m corresponds to the short axis of a half-magnitude profile of Gabor filters in the mth scale. $\Delta\omega$ represents the frequency bandwith in octaves. Movellan [30] proposes that there is a significant range in bandwidth ($\Delta\omega(\in [1, 1.5])$). $\Delta\phi$ denotes the half-magnitude orientation bandwith and β is fixed for Gabor functions in a certain frequency bandwidth. Implementing Fourier transformation for $G^e_{mk}(x, y)$, a_m can be derived as [30]:

$$a_m = \frac{\gamma\sqrt{2ln2}}{\sigma_m\pi} \tag{3.17}$$

Refer to Equation 3.15, it is obtained:

$$\sigma_m f_m = \frac{1}{\sigma\pi}\sqrt{\frac{ln2}{2}} \tag{3.18}$$

Based on Equation 3.17 and Equation 3.18, $\Delta\phi$ is reduced to:

$$\Delta\phi \approx 2arcsin(\frac{\gamma\sqrt{2ln2}}{2\pi\sigma_m f_m}) = 2arcsin(\gamma\beta) \tag{3.19}$$

Let N be the number of Gabor filters in a certain scale, $\Delta\phi = \pi/2N$ is satisfying. Consisting in Equation 3.19, the aspect ratio γ of the Gaussian envelope approximately equals to

$$\gamma \approx sin(\frac{\pi}{2N})/\beta \tag{3.20}$$

Therefore, given four parameters, namely, $\Delta\omega$ (the spatial-frequency bandwith), σ_1 (the biggest scale), M (the number of scales) and N (the number of orientations) are

enough to design an even Gabor filters bank. According to this, each Gabor bank is designed with Gabor filters in M scales and N orientations where $M = 1$, $N = 8$, $\Delta\omega = 1.12$ and $\sigma_1 = 8$. Based on the each Gabor filters bank, different transformed versions of a hand vein image are constructed by 2D convolution operation. The Figure 3.9 shows us the Gabor functions in Yang *et al.*'s [26] and their convolution wth hand vein images. Gabor filters bank and our proposed one, respectively. Besides, our proposed Gabor filters bank's functions and their convolutions are demonstrated in Figure 3.10.

3.3.2.2. Hand Vein Enhancement. In this procedure, we convolve the hand vein images with Gabor filters. As mentioned, we construct two Gabor filters banks both of which consists of different Gabor functions.

Let $R(x, y)$ be the hand vein image and $\hat{\mathbf{R}}(x, y)$ be its negative version and $E(x_i, y_i)$ be the enhanced hand vein image. $U_m^k(x, y)$ is the filtered result in even-symmetric Gabor transform domain. The relationship between $\hat{\mathbf{R}}(x, y)$ and $U_m^k(x, y)$ is:

$$U_m^k(x, y) = G_{mk}^e(x, y) * \hat{\mathbf{R}}(x, y) \tag{3.21}$$

where '*' denotes 2D convolution. We use $\hat{\mathbf{R}}(x, y)$ in convolution rather than $R(x, y)$ since the filters are more sensitive to white area. From now on, in order to construct an enhanced hand vein image, we use $M \times N = 8$ filtered images and select their maximum values.

Consider that $p(x_i, y_i)$ represent a point in $\hat{\mathbf{R}}(x, y)$ and S^i is the set of transformed filtered results of $p(x_i, y_i)$ in N different orientations an M different scales, S^i can be

represented as the set of filter bank outputs:

$$\begin{aligned} S^i &= \{U_1^1(x,y), ..., U_1^k(x,y), ..., U_1^N(x,y), \\ &\quad U_z^1(x,y), ..., U_z^k(x,y), ..., U_z^N(x,y), \\ &\quad U_M^1(x,y), ..., U_M^k(x,y), ..., U_M^N(x,y)\} \end{aligned}$$

$E(xi, yi)$ denotes the reconstructed image from $M \times N$ filtered results. In convolution, when a filter matches to a vein segment exactly, its convolution operation result becomes maximum among other filters' results. Therefore, $E(x_i, y_i)$ is defined as:

$$E(x_i, y_i) = \arg \max_{(U_z^k(x_i,y_i) \in S^i, i \in \Lambda)} (U_z^k(x_i, y_i)) \tag{3.22}$$

where Λ is an index set of the numbered pixels of $R(x, y)$. The last step is normalizing $E(x_i, y_i)$. To ensure that the outcome of enhanced hand vein image construction process will be a non-negative image pixel values of which are not more than one, we construct $\tilde{E}(x_i, x_i)$ image. $\tilde{E}(x_i, x_i)$ is the normalized version of $E(x_i, y_i)$ defined as:

$$\tilde{E}(x_i, y_i) = (E(x_i, y_i) - \eta)/(\epsilon - \eta) \tag{3.23}$$

where $\epsilon = \arg\max_{i \in \Lambda}(E(x_i, y_i))$ and $\eta = \arg\min_{i \in \Lambda}(E(x_i, y_i))$. As the result of the enhanced hand vein image construction process, we construct $\tilde{E}(x_i, y_i)$ for each hand vein image. $\tilde{E}(x_i, y_i)$ image is used for the input of converting a hand vein network to a graph process (See Figure 3.11).

3.3.3. Geometric Representation of Hand Veins

The outcome of the hand vein network enhancement process is a vein image in which the false vein information is mostly suppressed. In order to describe geometric representation of hand veins, we apply three consecutive processes to enhanced images which are binarization by Yasuda adaptive thresholding method, skeletonization, graph definition through LEM method.

3.3.3.1. Yasuda adaptive thresholding method. Since enhanced vein image is a gray-scale image, first, we need to binarize it into two classes as veins and background. According to Yuksel *et al.* [32], [1], we use Yasuda adaptive thresholding method.

Yasuda adaptive thresholding method first applies a normalization process, followed by a nonlinear smoothing which preserves the sharp edges. The smoothing based on replacing each pixel by the average of its eight neighbors if the local pixel range, the span between the local maximum and minimum values, is smaller than a threshold T_1. An adaptive threshold is applied in which the background (i.e., set to 255) is assigned to any pixel value if the local range is below a threshold T_2 or the pixel value is above the local average, both computed over bxb windows. If not, the dynamic range value is extended. Finally any pixel value is denoted as object point to be if its minimum over a 3x3 window is below T_3 or its local variance is above T_4. Thus:

$$B(i,j) = \begin{cases} 1, & \text{if } Ave_{(3x3)}I(i,j) < T_3 \text{ or } VarI(i,j) > T_4 \\ 0, & \text{otherwise} \end{cases} \tag{3.24}$$

where B is binarized image, I is hand vein image, Ave and $VarI$ are average and variance values, respectively.

3.3.3.2. Skeletonization. To form a graph from a hand vein structure, first we need to describe vein segments as graph nodes and graph vertices. Since a binarized vein image consists of vein segments in several widths and different diameters, we need to transform them into thin lines. Skeletonization is a process for reducing foreground regions in a binary image to extract a region-based shape feature representing the general form of an object whereby throwing away most of the original foreground pixels. There are many different algorithms for computing skeletons for shapes in digital images, such as using morphological operators, supplementing morphological operators with shape based pruning, using curve evolution, using level sets, finding ridge points on the distance function, "peeling" the shape, without changing the topology, until convergence. In this thesis, morphological operators are used for skeletonization of

hand veins through Matlab's "bwmorph" method. This method is operated with two options as "skel" and "thin". The former method removes pixels on the boundaries of objects but does not allow objects to break apart where The latter one only thins objects to lines. Since "skel" option does not let objects be split, it concatenates lines. These concatenations result in joint points in vein skeleton which can be confused with vein junction points. Owing to the fact that, "thin" option works more efficient while skeletonising hand vein segments. Figure 3.12 exhibits the difference between two options.

3.3.3.3. Graph definition through Line Edge Map (LEM). LEM is a method which decomposes the skeletonized vein patterns into a number of line segments. Gao *et al.* [33] proposed this algorithm for face recognition. They extract edge features from face images and constructed a LEM. Since the vein network already resembles a graph, this method is used in hand vein biometry, as well [9].

The algorithm works like this: First of all, junction points and end points in vein patterns are found. Then the algorithm searches the image and selects each vein pattern point as a starting point. From the starting point, it tracks in the edge direction by storing and labeling edge points. It continues until an end or junction point is encountered. At this point, the function returns to the starting point and track the edge in the opposite side. In the array of the edge list, the algorithm finds the size and position of the maximum deviation from the starting to the end point. If the maximum deviation is smaller than the specified deviation threshold(ts), the line is accepted. If not, the edge is divided in half. In this study we select two deviation thresholds as $ts = 2$ and $ts = 5$. For each line, this process is repeated till it is separated into lines all of which has smaller deviation than maximum deviation value. As the result, the starting and end points of current lines which are longer than length threshold ($tl = 10$) pixels are recorded to be used in graph construction.

In graph theory, unless stated otherwise, graph means "undirected simple graph"

defined as:

$$G = (V, E) \tag{3.25}$$

- V a set whose elements are called vertices or nodes
- E a set whose elements are called edges or lines

Literally, a graph is an abstract representation of objects (vertices) where some are connected by links (edges). Since LEM features are starting and end points of hand vein line segments, a hand vein graph can be formed by describing these points as graph vertices and the lines between these points as graph edges.

All steps on feature extraction module, namely, enhanced hand vein image, yasuda binarization, skeletonization, LEM form of the vein and graph definition through LEM are shown in Figure 3.13.

3.4. Identity Matching

Identity matching is the process in which the similarity of probe and test objects are calculated and the test object with the maximum similarity score is matched with the probe one.

In this thesis, similarity scores are calculated through Line Segment Hausdorff Distance (LHD), Modified Line Segment Hausdorff Distance (MLHD), Weighted Line Segment Hausdorff Distance (WLHD) and Graph Edit Distance (GED). Line segment based similarity measurement techniques strongly need a successful registration step. Thus, we construct a preprocessing step for line segment based similarity measurement which enhances ROI registration of test and probe objects.

3.4.1. Preprocessing Stages

Our first investigations show us that using uncontrolled captured hand vein images on a biometric system causes problems on ROI extraction. The lack of any hand docking device increases the probability of wrongly extracted ROIs. Geometric approaches are remarkably influenced by spatial differences of the same line segments in different ROIs. Due to this, we optionally apply two different registration enhancement methods on the hand vein ROIs before measuring their similarity. The first method is based on selecting keypoints whereas the second one is based on extracting LEM from each hand vein structure, iteratively.

3.4.2. Optional Preprocessing 1: Enhancing registration with keypoints

Keypoints are the important points in the images. Homologous keypoints in two images denote us the same physical points under different illuminations or positions. In this section, keypoints are used for registration of two hand vein ROIs. We first match them and align the ROIs with Procrustes analysis [34], [35] on the base of these matched keypoints.

Matched keypoints are constructed in three steps namely, keypoint detection, descriptor extraction and keypoint matching. For keypoint detection, hand vein junctions and SURF interest point detectors [36], [37]; for descriptor extraction, SURF interest point descriptor [36], [37] are used. Finally, we match them with Euclidean distance metric.

3.4.2.1. SURF: Speeded-up Robust Features. Speeded-up Robust Features (SURF) is a method that we can use on both keypoint detection and descriptor extraction. It is first proposed by Bay *et al.* in 2006 [36] and detailed in 2008 [37]. SURF algorithm consists of the main parts which are described below:

SURF Interest Point Detection: An interest point in an image has significant

properties which make it stand out when it is compared to its neighbouring points. Selecting interest points from the points which represent corners in an image is a feasible way. These corner points can be detected by calculating the second partial derivatives or candidate points, by applying Hessian matrix. Instead of doing this, SURF simplifies Hessian matrix usage with the helps of integral image and box filters, and gains speed.

Interest points may appear in different scales. In order to detect these points, integral image and box filter approaches are applied on different scales of the target image. After that, the detected points are compared to its neighbours by non-maxima suppression. If the point's non-maxima suppression response is bigger than all other neighbors' responses, the point is classified as interest point.

SURF Interest Point Description: SURF interest point description is pursuant to interest point orientation assignment and descriptor calculation. Orientation assignment is done by Haar wavelet filters in x and y directions. The orientation of an interest point is affected by its neighbours. In a radius s, the orientations of each neighbour is calculated. After that, calculated orientations are mapped to a new space where the x direction response is the abscissa and y direction response is ordinate. In $\frac{\phi}{3}$ neighbouring in new scale, the vector which described by the maximum number of orientations assigned to interest point. The x parameter of assigned orientation is called as d_x where the y parameter is called as d_y. According to d_x and d_y values, the 64 dimensional descriptor vector is extracted by concatenating four dimensional descriptor vectors each of which has 16 regions.

3.4.2.2. Procrustes Analysis. Procrustes analysis is proposed by Gower [34] to analyse the geometrical shapes in a statistical approach [35]. When a figure is affected from any translation, rotation or scaling operation there still exists many unchanged geometrical features belong to this shape. These characteristics are called as the *geometrical shape*. If a geometrical shape in R^N is labeled with l landmarks, it can be represented with a lxN matrix P. Each row in P matrix represents one of the labeled l landmarks in N

dimension.

Let $P : l\text{x}N$ and $P' : l\text{x}N$ be the matrices of two figures. These figures have the same shape if they have a similarity transformation as given below:

$$P' = \beta P\Gamma + 1_l\gamma^T \tag{3.26}$$

where $\Gamma : N\text{x}N, |\Gamma| = 1$ standing for the rotation, $\gamma : N\text{x}1$ standing for the translation, β standing for a positive scale constant, and 1_l defining a vector of ones. According to this equation, shape P is mapped to P' by appropriate translation, rotation and scaling transformations.

An example for Procrustes analysis is given in Figure 3.14.

3.4.2.3. Aligning two ROIs by using SURF and Procrustes Analysis. There are two subparts in ROI alignment; keypoint detection and description, and keypoint matching. The matched keypoints are accepted as input landmarks of Procrustes Analysis.

Keypoint detection and description: As it is mentioned, we define two different ways for selecting and describing keypoints of hand vein structures that are described as follows:

(i) For a hand vein ROI, we first convert it to a graph form by using LEM method. Junction points in this graph are selected as keypoints. Afterwards, SURF descriptors are extracted from enhanced ROI by using these junctions' spatial information.
(ii) For a hand vein ROI, SURF interest points are selected as keypoints and SURF descriptors are extracted from them.

Both ways give us keypoint descriptions that we use in keypoint matching.

Keypoint matching: Generally, matching techniques have similar mechanisms.

They use a similarity metric for comparing subjects pursuant to previously defined threshold value. If compared subjects' similarity score is lower than threshold, matching is not successful. If not, they are accepted as homologous pairs. This method does not ensure that each matching will be in one-to-one correspondence. However, for Procrustes alignment, each landmark has to be paired with exactly one element of the other landmark set. To satisfy this property, we apply an adaptive threshold selection algorithm while matching hand vein keypoints.

For matching keypoints, our adaptive threshold selection algorithm uses Matlab's matchFeatures method with "sum of absolute differences (SAD)" similarity measurement metric option. This matching function accepts a threshold scalar greater than 0 and less than or equal to 100. According to our experiments, we notice that best initial threshold value is 5. Since increasing this value returns more matches, we adaptively decrease this value until every match set has one-to-one matching pairs.

As the result of this process, we get a set of one-to-one matched keypoints from compared ROIs. By using these keypoints we align the graph forms of hand vein structures rather than aligning ROIs. Owing to this, we prepare modified graph inputs for identity matching module.

3.4.3. Optional Preprocessing 2: Enhancing Registration by Iterative LEM

Iterative LEM method is modification of an extracted LEM by the reference of most similar line segment. Based on the reasons, explained in Section 3.4.2, we attempt to find a method to coincide the compared hand vein structures more precisely. Iterative LEM is another optional method designed for this purpose.

Iterative LEM method has a restriction that, it has to be used with a line segment similarity measurement metric. The process is as follows: Let LEM (a) and LEM (b) be two LEMs to be compared. The most similar line segments between these LEMs is selected by a line segment measurement method. In order to map the selected line of LEM (a) to the selected line of LEM (b), appropriate translation, rotation and scaling

transformations are calculated. Then LEM (a) is altered by these transformations. The assumption behind this idea is that, if compared LEMs are the same hand's data, the most similar line segments will belong to the same hand vein segment. We aim to coincide the two LEMs by fitting one selected line to another.

For a hand vein segment in two LEMs, it is possible that the extracted line's length can be different. To overcome this problem, we iterate the coincided LEMs by translating one line on another. We decide to translate the lines by a step size of 5. After each iteration the similarity score between two LEMs are calculated and the minimum one is accepted.

3.4.4. Line Segment Hausdorff Distance (LHD)

Hausdorff distance (HD) is a measurement metric used to compare similarity of sets and shapes. Unlike most of the shape comparison methods, it does not need to build a one-to-one correspondence between the model and test images. LHD is an extension of HD which is used for comparing line segments. In addition to HD, it incorporates with the local structure of information such as orientation and line-point association of the images and is also sensitive to outlier lines.

LHD measures the dissimilarity (distance) of two sets (model and test sets) which consist of line segments. These line segments are defined by start and end points and LHD calculates the dissimilarity of two sets by using these points. Suppose that $M^l = m_1^l, m_2^l, ..., m_p^l$ represents a model set which has p lines and $T^l = t_1^l, t_2^l, ..., t_q^l$ represents the test set with q lines where l stands for line. The dissimilarity between m_i^l and t_i^l lines is defined by vector $d^{\rightarrow}(m_i^l, t_j^l)$ which can be represented as:

$$\begin{bmatrix} d_\theta(m_i^l, t_j^l) \\ d_\parallel(m_i^l, t_j^l) \\ d_\perp(m_i^l, t_j^l) \end{bmatrix} \tag{3.27}$$

where $d_\theta(m_i^l, t_j^l)$, $d_\parallel(m_i^l, t_j^l)$ and $d_\perp(m_i^l, t_j^l)$ are angle distance, parallel distance and

perpendicular distance, respectively. All these three distance types are independent and defined as:

$$\begin{aligned} d_\theta(m_i^l, t_j^l) &= tan(\Theta) \\ d_\parallel(m_i^l, t_j^l) &= min(l_{\perp 1}, l_{\perp 2}) \\ d_\perp(m_i^l, t_j^l) &= l_\perp \end{aligned} \tag{3.28}$$

To illustrate $d_\parallel(m_i^l, t_j^l)$ and $d_\perp(m_i^l, t_j^l)$ distances, Figure 3.15 is used. According to the above dissimilarity measurements, the distance between the two line segments m_i^l and t_j^l is:

$$d(m_i^l, t_j^l) = \sqrt{(W_a d_\Theta(m_i^l, t_j^l))^2 + d_\parallel^2(m_i^l, t_j^l) + d\perp^2((m_i^l, t_j^l))} \tag{3.29}$$

where W_a weight for angle distance. Pursuant to Yuksel *et al.* [1], we set W_a to 20 in this study. For calculating $d(m_i^l, t_j^l)$ this sequence is followed: First, $d_\Theta(m_i^l, t_j^l)$ is measured. Secondly, the shorter line rotated and two lines become parallel. Lastly, $d_\parallel^2(m_i^l, t_j^l)$ and $d\perp^2((m_i^l, t_j^l)$ are calculated and using these three distances $d(m_i^l, t_j^l)$ is measured. After that, LHD is defined as:

$$h(M^l, T^l) = \frac{1}{\sum\limits_{m_i^l \in M^l} l_{m_i^l}} \sum_{m_i^l \in M^l} l_{m_i^l} \cdot \min_{t_j^l \in T^l} d(m_i^l, t_j^l) \tag{3.30}$$

$$H_{LHD}(M^l, T^l) = \max(h(M^l, T^l), (T^l, M^l)) \tag{3.31}$$

where $l_{m_i^l}$ is the length of the line segment m_i^l.

3.4.5. Modified Line Segment Hausdorff Distance (MLHD)

MLHD similarity measurement is designed for tolerating small differences on registration process. The only difference between LHD and MLHD measurement metrics is the parallel distance. MLHD measures parallel distance between two line segment

the same as LHD unless one of these two lines cover the other line. If this occurs, parallel distance is accepted as 0. Figure 3.16 shows the conditions in which the parallel line is accepted as zero.

3.4.6. Weighted Line Segment Hausdorff Distance (WLHD)

In a hand vein image, the visibility of thick and superficial vein segments are more obvious than deeper and thin ones. This is also shown in enhanced hand vein image ($\tilde{E}$) as the former vein segments' intensity values are higher than the latter ones. The obviousness of weak veins in an image are overcome by illumination and hand posture compared to strong ones. This gives us the idea that, when comparing two hand vein images, the lack of obvious vein segments can guide us more than not existing weak vein segments. According to these, we modify LHD method on the basis of the intensity values of the lines. By calculating an intensity weight for each line of the hand vein LEM, we measure dissimilarities of two different hand vein images. For calculating weights, we utilize enhanced hand vein images.

Suppose that $M^l = \{m_1^l, m_2^l, ..., m_p^l\}$ represents a hand vein LEM which has p lines and $\tilde{E_M}$ is the enhanced hand vein image corresponding to M_l. Each line m_i^l in the set of M^l consists of a number of points defined as:

$$m_i^l = \{a_1^i, a_2^i, ..., a_p^i\} \tag{3.32}$$

where $a_j^i = (x_{a_j^i}, y_{a_j^i})$ stands for the pixel coordinates of a point on the m_i^l line. According to this, intensity weight of m_i^l is defined as:

$$w_{m_i^l} = \frac{1}{lm_i^l} \cdot \sum_{aj \in m_i^l} \tilde{E}(a_j^i) \tag{3.33}$$

Suppose that $W^l = \{w_1^l, w_2^l, ..., w_p^l\}$ represents the weight set of M^L where w_i^l shows the weight attribute of m_i^l line. To achieve consistency in dynamic range for line weights

of each LEM, we normalize the weights according to this rule:

$$w_i^l = (((w_i^l - \eta)/(\epsilon - \eta)) * (1 - a) + a)^{(1/b)} \tag{3.34}$$

where $\epsilon = \arg\max(W^l)$, $\eta = \arg\min(W^L)$ and a and b are the parameters to change the effect of weights. This similarity metric is tested on hand vein images by using different a and b parameters. The results of these tests are given in Section 4.3. To adapt LHD to WHD, we modify $h(M^l, T^l)$ calculation as:

$$h(M^l, T^l) = \frac{1}{\sum\limits_{m_i^l \in M^l} l_{m_i^l}} \sum_{m_i^l \in M^l} l_{m_i^l} \cdot w_i^l \min_{t_j^l \in T^l} d(m_i^l, t_j^l) \tag{3.35}$$

where $H_{LHD}(M^l, T^l)$ calculation stays the same as the LHD method.

3.4.7. Graph Edit Distance (GED)

Since exact graph matching is not possible in a real world application, there is a need for error tolerant and error correcting metrics. GED is a graph similarity measurement technique commonly used in real world graph matching or similarity calculating applications. Assume that we have two graphs G and G'. GED is the least cost of operators used to simulate graph G to G' [38].

The operators used for the GED calculation process are in an application-specific way. However, the six main operators which are mostly used in a GED calculation are node insertion, node deletion, node substitution, edge insertion, edge deletion and edge substitution. For simulating graph G to G', first a seed node has to be selected from the graphs to perform the algorithm. Seed node selection operation varies, depending on the needs of the GED algorithm. For example, it is possible to choose the seed nodes from both graphs one by one, randomly or according to node features' similarity.

To illustrate the GED calculation algorithm for an exact matching, we demonstrate it on the graphs given in Figure 3.17, top image, graph G and bottom image,

graph G'. To simulate graph G to G':

- We select seed nodes from both graphs. Suppose that 3s in both graph are selected as seed nodes.
- The required changes on graph G
- Node 5 is inserted.
- A new edge is inserted between node 5 and node 3.
- The edge between node a and node 1 is deleted.
- The edge between node a and node 4 is deleted.
- Node a is deleted.
- Node 6 is added.
- A new edge is inserted between node 4 and node 6. (It is important that, in order to delete a node we have to delete its edges first.)
- Above operations are enough to simulate graph G to G'. In order to calculate GED of this simulation we need to know cost of each GED operation. If we accept that all GED operators have the same cost C, GED to simulate graph G to G' is 7*C.

3.4.7.1. GED in Biometric Verification. GED has been used in different biometric verification application. Bunke *et al.* [39] used GED to classify fingerprint images. They classified fingerprints according to the Henry System, namely arch, tented arch, left loop, right loop and whorl and assigned the same number of fingerprint graphs to each of the five classes. In order to convert fingerprint images to fingerprint graphs, they first obtained an averaged ridge orientation field from each image and separated this field to small squares. After that, they obtained a graph from each field by converting each square to labeled nodes and converting each vector between squares to edges, by protecting their tangent values. Finally the graphs are compared by their Approximate Graph Edit Distance metric (AGED) and each fingerprint is substituted to its most similar fingerprint type. Bunke *et al.* [40] modified their algorithm by defining two new operators as node merging and node splitting. The aim of these operators is to tolerate the errors of image processing operations and prevent these errors to mislead

GED algorithm. The images captured at different times from the same person could be different because of environmental factors. When these images are converted to graphs, differences in images can cause more or fewer node and edge generation. In order to avoid this, before performing GED algorithm the graphs are compared and required splitting or merging operations are done. To the best of our knowledge, no public hand vein biometric verification system is supplied presently which uses GED metric for similarity calculation between two hand vein graphs. Since a hand vein graph consists of considerably small size of nodes and edges, calculating GED is more suitable to hand vein graphs rather than AGED. As it is described, to apply GED metric we first need to select seed nodes from both graphs. One disadvantage of selecting seed nodes randomly is increasing run time due to the fact that it calculates all candidate GEDs and chooses the smallest one. To avoid this, we select seed nodes most similar seed nodes from the graphs as starting points and traversed the graph until depth of two. Besides, we make applicable to select more than one seed node for one graph that helps to tolerate misleading information on graphs.

3.4.7.2. Seed Node Substitution Method. In image acquisition, environmental factors can affect the quality of the image and make the veins less visible. However, a vein junction point, a connection points of 3 different veins, is affected from these factors less than other vein points. So, we developed an algorithm to substitute junction points in graph G and G' and use them as seed nodes for the GED algorithm.

First of all, we selected a junction node J from graph G and found the Euclidean distance between this junction point and all junction points in graph G'. If the distance between junction J and any junction point in G' is less than a threshold value, we constructed a candidate substitutions set for junction J with these junction nodes in G'. After that, we looked at the angles between the junction nodes and their three edges. The candidate junction node which has the nearest angle values to junction J's angles is selected as the substitution node of junction J. Simpler graphs are easier to match. So, we investigated graph G and G' from the junctions to a neighbourhood depth of two. After matching, we replaced all investigated edges and nodes as a complex node

on the graph. Thus, we simplified graphs G and G' by decreasing the number of nodes and edges. For example:

- Graph G has node 1 which is the neighbours of node 2, node 3 and node 4.
- Node 2, node 3 and node 4 are the neighbours of node 5, node 6 and node 7, respectively.
- Assume that node 1 is selected as a seed node in graph G and none of the nodes 1 to 7 is a junction node. If there is no need for any change on graph G while traversing from node 1 to two neighbours depth, graph G is updated adding a complex node 1, and node 1, node 2, node 3, node 4 and their edges are deleted from graph G and node 5, node 6 and node 7 become the new neighbors of 'complex' node 1.

3.4.7.3. Calculated GED through Simplified graphs G and G'. At this stage, we investigated all nodes and edges in graph G and G' without any depth control. In a hand vein graph, the graph mostly consists of more than one sub graph. Thus, in order to traverse each node and edge, we firstly assigned corresponding sub graphs in graph G and G' and investigated the graphs through their sub graphs. We used two methods to substitute sub graphs:

(i) If the sub graph S in G has a complex node C, there is a previously assigned substitution C' for C in sub graph S' in graph G'.
(ii) If there are no complex nodes in sub graph S, we calculated the weighted average of sub graph S and sub graph S' in G' which has the nearest weighted average to S substituted to S'.

- To traverse whole G and G', we need to select seed nodes from the sub graphs, as well. If selected sub graph S in G is substituted by the first method, its complex node and its substitution are selected as seed nodes. If the second method is used for sub graph substitution, we substitute more similar nodes in S and S' on the basis of the angle similarity of their edges and select them as seed nodes for sub

graphs.

- Finally, by comparing each sub graph in G with its substitution sub graph in G', we calculated GED of graph G and G', which gives us a cost to match graph G to G'.

3.4.7.4. Demonstration of the GED Algorithm on an Example. In the example shown in Figure 3.18, graph G and G' both consist of one sub graph. However a hand vein graph can consist of more than one sub graphs. Let us calculate the GED to match Graph G (Figure 3.18a) and G' (Figure 3.18b):

(i) Node 6, node 10, node 14, node 19, node 22 and node 23 in graph G are substituted to node 8, node 10, node 13, node 19, node 23 and node 24 in graph G', respectively.

(ii)
- Counter-clockwise neighbours of Node 6 in graph G: 7, 20, 14
- Counter-clockwise neighbours of Node 8 in graph G': 9, 21, 18
- For the case that Node 6 in graph G and Node 8 in Graph G' are selected as seed nodes, after the investigation until 2 neighbourhoods depth, the changes in graph G:
  (i) The edge between node 6 and node 14 is deleted.
  (ii) Node 27 is added.
  (iii) Node 27 is substituted with node 18 in graph G'.
  (iv) An edge is added between node 6 and node 27.
  (v) An edge is added between node 27 and node 14. In this algorithm, we accepted that substitution operator is costless and other operators have the same cost C. Thus, GED of the above operation is $4 * C$.

(iii) Second step is repeated for other substituted seed nodes.

(iv) After all seed nodes are traversed until 2 neighborhoods depth, graph G is converted to third row, first column image and graph G' is converted to third row, second column image.

(v) Simpled graph G and graph G' are traversed through subgraphs without any depth restriction. Since node 8 does not have any substitution in graph G', it is

Table 3.1. The seed nodes of the graphs and calculated GED through these seed nodes.

The seed node in graph G	The seed node in graph G'	GED
10	10	0
14	13	$3 * C$
19	19	$4 * C$
22	23	0
3	24	$2 * C$

deleted from graph G.

(vi) Total GED value is calculated as $(4 + 3 + 4 + 2 + 1) * C = 14 * C$.

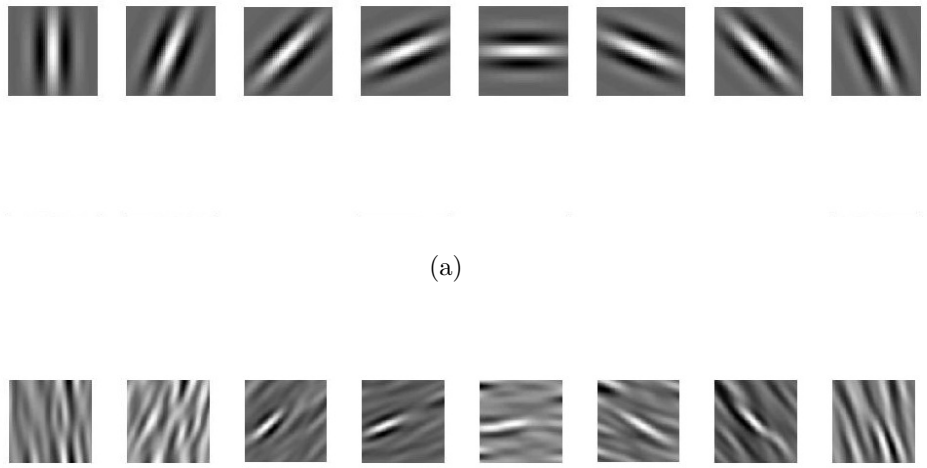

(a)

(b)

Figure 3.9. (a) 2D spatial filters of Yang *et al.*'s [26] even-symmetric Gabor bank, (b) their convolution results.

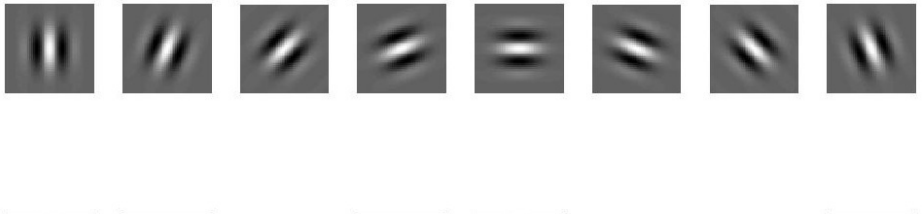

(a)

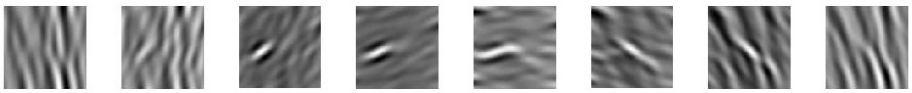

(b)

Figure 3.10. (a) 2D spatial filters of our proposed even-symmetric Gabor bank, (b) their convolution results.

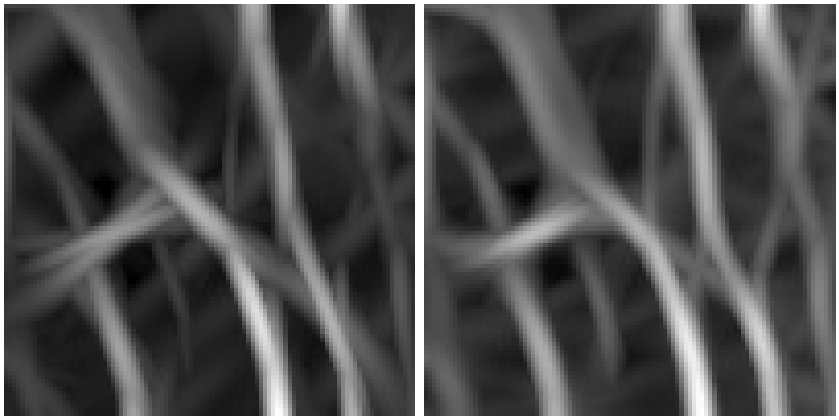

(a) (b)

Figure 3.11. Enhanced vein images yielded by (a) Yang *et al.* [26] Gabor filters bank, (b) Our proposed Gabor filters bank.



(a) (b) (c)

Figure 3.12. Skeletonization of vein segments (a) Vein Image, (b) Skeletonization by "skel" option, (c) Skeletonization by "thin" option.

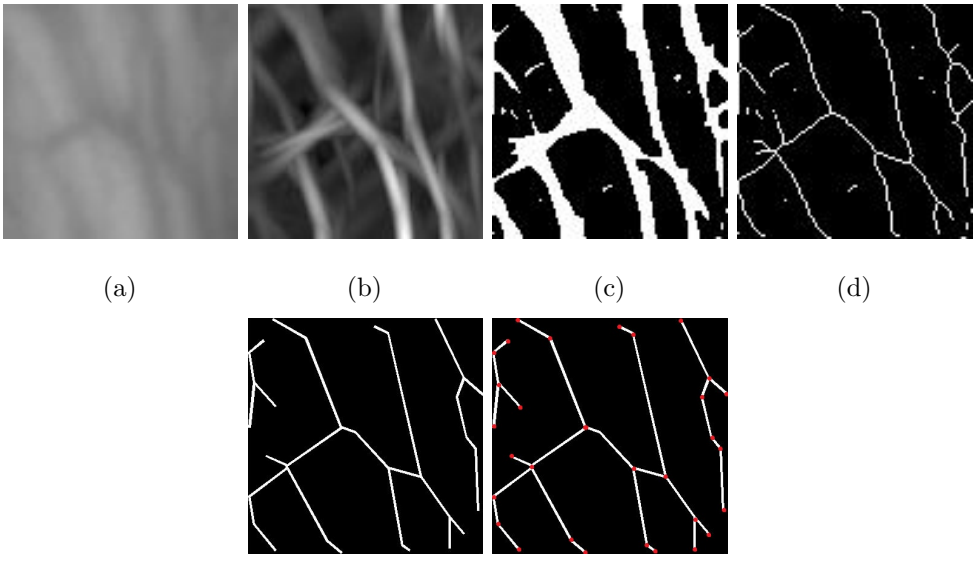

(a) (b) (c) (d)

(e) (f)

Figure 3.13. Feature extraction steps: (a) Hand vein ROI image, (b) Enhanced hand vein image by even-symmetric Gabor filters bank, (c) Yasuda binarization, (d) Skeletonization, (e) LEM, (f) Graph definition of LEM where each red points represent node and white lines stand for edges.

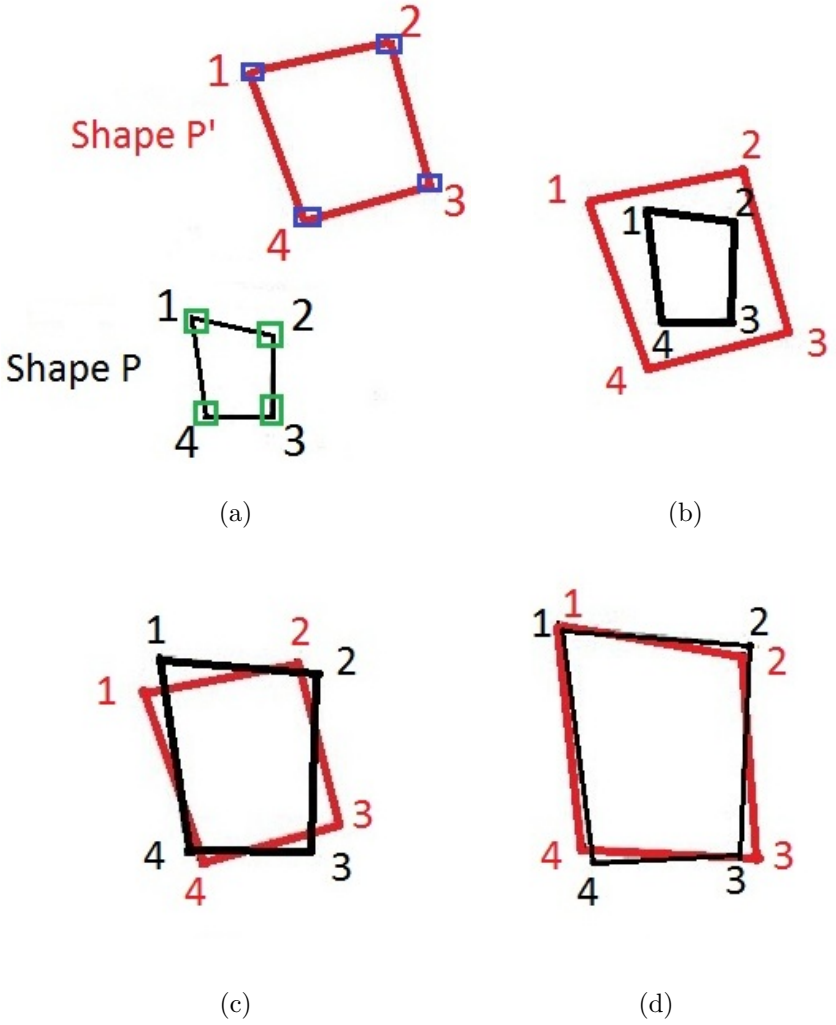

Figure 3.14. Three steps of Procrustes analysis: (a)Raw figures and their landmarks, (b)Translation to centroids, (c) Scaling, (d) Rotation.

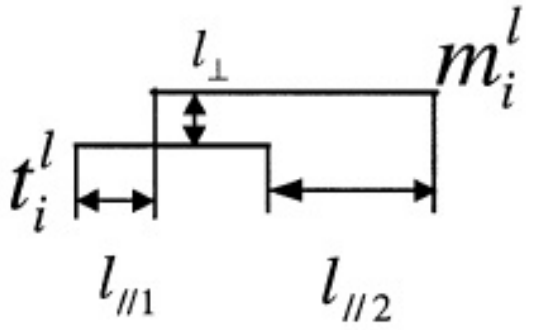

Figure 3.15. $d_\parallel(m_i^l, t_j^l)$ and $d_\perp(m_i^l, t_j^l)$ dissimilarity measurements.

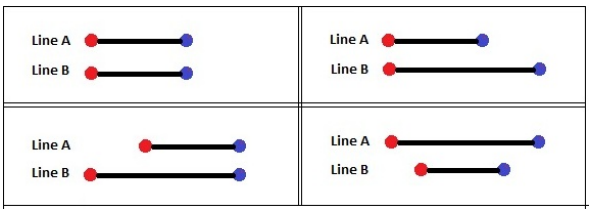

Figure 3.16. MHLD conditions in which parallel distance is accepted as 0.

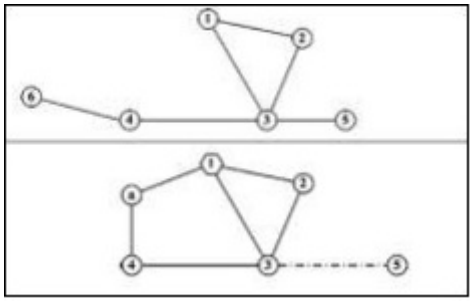

Figure 3.17. Top: graph G' bottom: graph G.

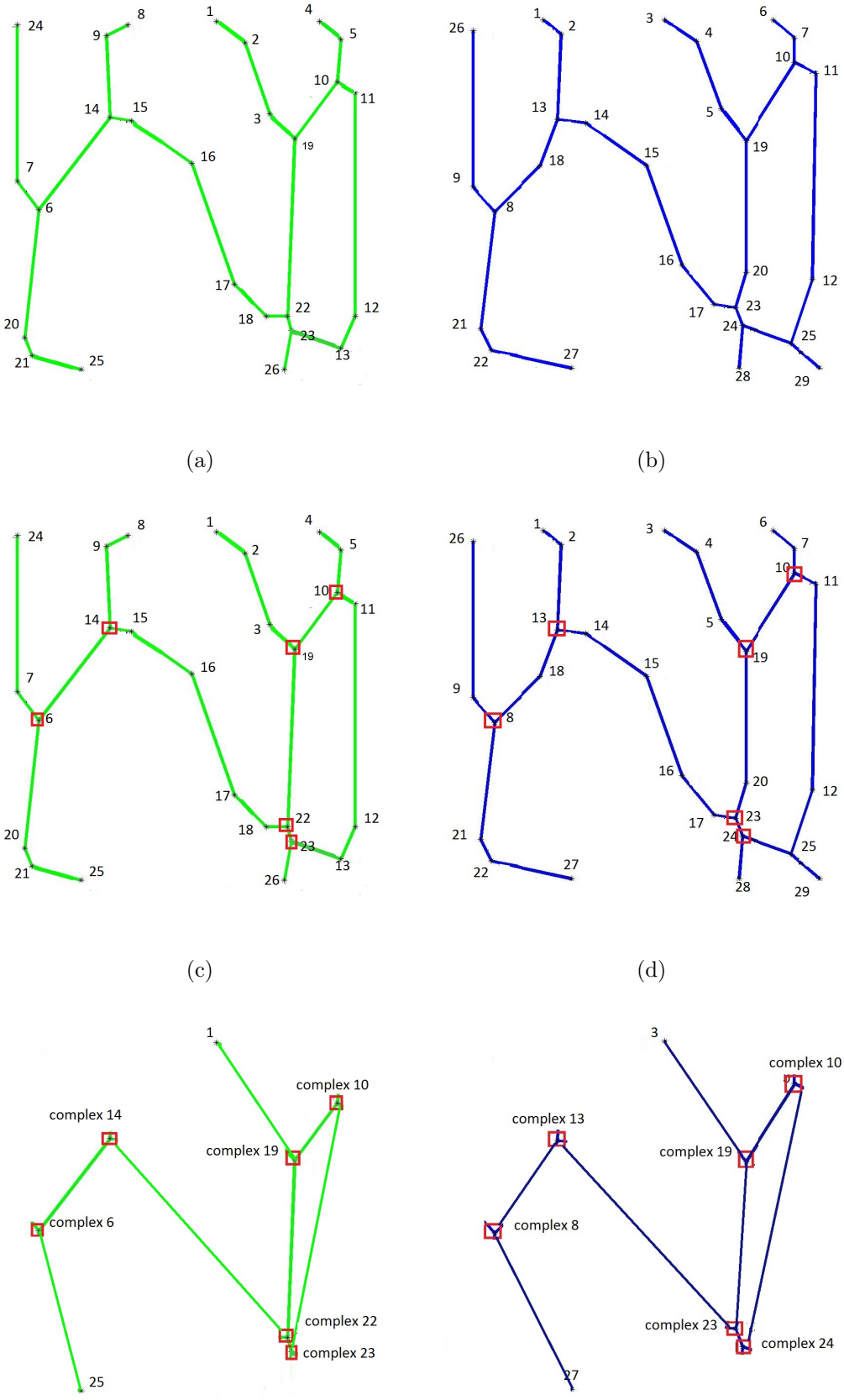

Figure 3.18. Changes in graph G and G' while perfoming GED algorithm.

4. EXPERIMENTS

In this thesis, we propose a set of geometric approaches to hand vein biometry and test them on the Bosphorus Hand Vein Database, which we describe in Section 4.1. In this section the scope of the experiments, obtained results and inferences from these experiments are given implicitly.

4.1. Dataset

The prior studies on hand vein biometrics collect their own hand vein datasets or use one of the publicly available datasets such as CASIA Multi-Spectral Palmprint Image Database (CASIA database) [41], TJU hand vein database [42], and PolyU Multispectral Palmprint Database (PolyU database) [43]. In this study, we work on Bosphorus Hand Vein Dataset [32], [1] which is open to researchers.

Bosphorus Hand Vein Dataset has been collected by NIR infrared imaging technique based on reflection method. The image acquisition setup, which can be schematically seen in Figure 4.1, consists of a monochrome NIR CCD camera, two IR light sources and diffusing paper. The hand vein images are captured in a dark environment in order not to be affected by visible lights. Subjects place their hand on the black background such that the back side of the hands are visible to the camera. Hands are captured in a relaxed, arbitrary hand positions with all the fingers visible. As the result of the deinterlacing processes, Bosphorus Hand Vein Dataset is constructed by 300x240 grey level hand vein images. The images are collected from left and right hands of 120 subjects. While acquiring the images, samples are taken under different conditions to simulate the effects of physical conditions of hand veins. The left hand images are captured in four dissimilar conditions [1]:

- Under normal condition (N: Normal),
- After having carried a bag weighing 3 kg. for one minute (B: Bag),
- After having squeezed an elastic ball repetitively (closing and opening) for one

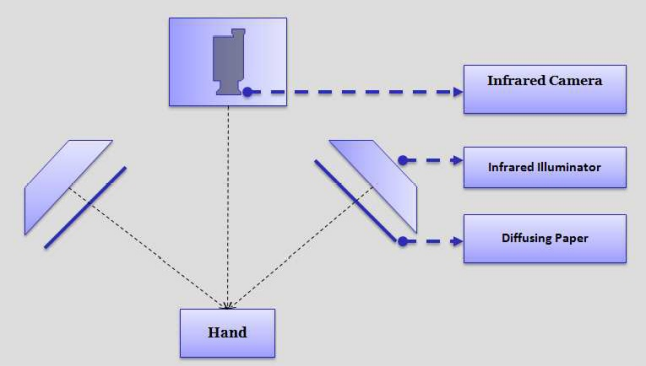

Figure 4.1. Camera setup of Bosphorus Hand Vein Dataset obtained from [1].

Table 4.1. Dataset Information obtained from [1].

Gender	Female: 42 person, Male: 58 person
Left or Right Handed	Left: 2 person, Right: 98 person
Age	Varying between 16-63

minute (Activity: A),

- After having cooled the hand by holding an ice pack on the surface of the back of the hand (Ice: I).

For each condition, three images are captured, resulting in 12 ($3*4$) images per subject for the left hand. The right hands of the subjects are also captured, but only under normal conditions, resulting in three images per subject for the right hand. In order to inspect the effects of time on hand veins, left hand images have been collected from 25 subjects under normal conditions after some time delay ranging from two months to five months.

The dataset consists of the data of 42 female and 58 male subjects who are in a large age range. The properties that belong to volunteer subjects, are given in Table 4.1 in detail.

4.2. Methodology

4.2.1. Recognition, Identification and Verification

A biometric system relies on the recognition of a person by his/her characteristics or traits. A biometric system has to answer one of these two questions: "who am I?" or "am I who I say I am?". In other words, if a system identifies a subject by comparing him against the previously collected subject samples, it attempts to find an answer to the "who am I" question. These kind of systems are used for identification purposes. Secondly, if a system verifies that a subject is who he/she claims to be by comparing it against previously collected data, , it aims to respond to the "am I who I say I am?" question. These systems are called as verification systems.

In this work, we test our system in both identification and verification modes. In the identification mode, the user does not assert any identity claim in our system. The system checks the database and reveals the identity of the user against the previously enrolled users hand vein data. We measure the similarity of the user's hand vein features with each subject's features in the database. Then, the subject who has the maximum similarity score with the user is accepted as who the user is. If we run a system in the verification mode, the system aims to compare the user with a specified similarity threshold to decide whether he/she is an impostor or a genuine user. This differentiation is done as follows: The features of the user and his/her claimed identity are compared by a similarity metric and if the similarity score is below the threshold, the user's assertion is rejected. If the similarity score is above the threshold, then the user is accepted as his/her claimed identity.

4.2.2. Performance Measures

For identification tests, identification rates (IR) are used and for verification tests, equal error rates (EER) are calculated.

4.2.2.1. Identification Rate (IR). IR is the ratio which is attained by dividing the number of true classified test subjects to the number of all test subjects.

4.2.2.2. Equal Error Rate (EER). EER is the rate at which both false accept and false reject rates are equal. In general, the accuracy of the system is inversely proportional to EER. In other words, more accurate biometric systems have lower EER rates.

4.3. Experimental Setup

4.3.1. Enrollment and Test Sets

In order to assess the success rates of our proposed methods, we construct an experimental setup consisting of several tests. These tests are applied to the Bosphorus Hand Vein Database. In this database, there are 120 subjects and both hands of each subject are captured. We are only interested in left hand vein images of 100 subjects.

In the Bosphorus Hand Vein Database, left hand vein images of each subject are captured in four different conditions: normal, after carrying bag, after an activity, and after having cooled the hand with ice. In further sections, these conditions are denoted as N, B, A, I, respectively. Moreover, each hand is recorded three times for each condition. Thus, 1, 2, and 3 numbers are postfixed. For instance, all left hand vein images captured under normal conditions at the first recording session are denoted as N1.

Each subject has to authenticate himself/herself to the system by enrolling his/her biometric data before using it. Hence, we need the enrolled hand vein image of each person who is to be tested. In our experiments, we select the enrolment and test datasets as given in Table 4.2 and Table 4.3.

Each test is run on the given dataset pairs. For calculating the result of an experiment for any condition, we use the average value of all tests for any given test

Table 4.2. Enrolment and test set pairs of single enrolment for each condition.

Enrollment	**Test**	**Test type**
N1	(N2,N3)	Normal
N2	(N1,N3)	
N3	(N1,N2)	
N1	(A1,A2,A3)	Activity
N2	(A1,A2,A3)	
N3	(A1,A2,A3)	
N1	(B1,B2,B3)	Bag
N2	(B1,B2,B3)	
N3	(B1,B2,B3)	
N1	(I1,I2,I3)	Ice
N2	(I1,I2,I3)	
N3	(I1,I2,I3)	

Table 4.3. Enrolment and test set pairs of double enrolment for each condition.

Enrollment	**Test**	**Test type**
(N1,N2)	N3	Normal
(N2,N3)	N1	
(N1,N3)	N2	
(N1,N2)	(A1,A2,A3)	Activity
(N2,N3)	(A1,A2,A3)	
(N1,N3)	(A1,A2,A3)	
(N1,N2)	(B1,B2,B3)	Bag
(N2,N3)	(B1,B2,B3)	
(N1,N3)	(B1,B2,B3)	
(N1,N2)	(I1,I2,I3)	Ice
(N2,N3)	(I1,I2,I3)	
(N1,N2)	(I1,I2,I3)	

condition.

We design eight experiments on these enrolment and test set pairs:

4.3.1.1. Experiment 1: Registration by warping. It is designed to improve registration of hand image pairs and applies TPS warping (Section 3.2.2.1) on enrolment and test sets. New sets are passed from LEM extraction procedure, and similarity scores are measured by MLHD method. In order to see the success rate of the warping process, the results are compared with Yuksel *et al.*'s work [1] which uses the same methods. The results for single enrolment is presented in Table 4.4.

It can be easily noticed on the given results that warping operation decreases the success rate. Data inspection shows us that hand segmentation algorithm cannot locate finger valleys exactly. The finger valleys of a person's hand can be located differently in two different images (Figure 4.2 illustrates an example.). This causes a

Table 4.4. MLHD measurement of warped images for single enrolment.

Set	**Rate**	**Warped Images**	**Yuksel *et al.* [1]**
Normal	IR	56.00	**68.50**
	EER	19.31	13.52
Activity	IR	60.00	**71.77**
	EER	19.34	12.76
Bag	IR	61.00	**73.77**
	EER	17.57	12.13
Ice	IR	54.77	**65.77**
	EER	18.89	14.07
All	IR	57.94	**69.95**
	EER	18.77	13.12

negative deformation on warped images since we map differently located valleys with homologous points. Furthermore, while mapping an area to another one, selecting reference points near to this area increases the effectiveness of the warping. We notice that, in the course of capturing an uncontrolled hand vein image, the most specific changes are seen near the wrist area. As our reference points are from the top side of the hand, even if we have correctly located reference valley points, warping may not bring an advantage.

4.3.1.2. Experiment 2: ROI Enhancement. This experiment is designed to see the effects of Gabor filters banks and LEM thin slope parameter selection. The enrolment and test sets are provided as inputs to these selection sets:

(i) Gabor filters bank Equation 3.13 and LEM with thin slope $ts = 2$.
(ii) Gabor filters bank Equation 3.13 and LEM with thin slope $ts = 5$.
(iii) Gabor filters bank Equation 3.14 and LEM with thin slope $ts = 2$.
(iv) Gabor filters bank Equation 3.14 and LEM with thin slope $ts = 5$.

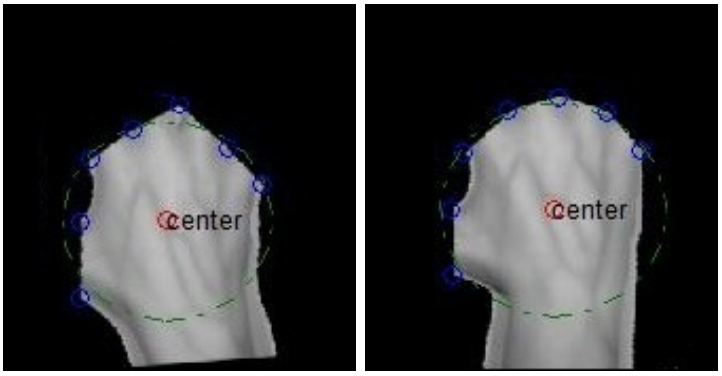

Figure 4.2. Two hand vein images captured from the same hand. The finger valleys, especially the valleys near of the middle and ring finger are dissimilar.

The extracted hand vein features are measured by MLHD. The Table 4.5 and Table 4.6 show the results of single and double enrolment sets, respectively.

Table 4.5. MLHD measurement for single enrolment with different Gabor filters banks and LEM parameters.

		Gabor filters Bank Eq 3.13		**Gabor filters Bank Eq 3.14**		**Yuksel *et al.* [1]**
Set	**Rate**	**ts = 2**	**ts = 5**	**ts = 2**	**ts = 5**	**ts = 2**
Normal	IR	69.00	68.16	**73.00**	68.50	68.50
	EER	15.16	15.37	11.99	13.16	13.52
Activity	IR	71.88	68.11	**74.33**	72.44	71.77
	EER	12.89	13.77	11.88	11.66	12.76
Bag	IR	**72.55**	72.11	**72.55**	71.00	73.77
	EER	12.47	11.66	12.54	12.52	12.13
Ice	IR	66.55	63.11	**67.00**	64.88	65.77
	EER	15.66	16.69	14.66	13.97	14.07
All	IR	69.98	67.87	**71.72**	69.20	69.95
	EER	14.04	14.37	12.76	12.82	13.12

We observe that the third scheme, that is, using Gabor filters bank of Equation 3.14 and LEM with thin slope $ts = 2$ gives best results for single and double enrolment. Inspection from Figure 4.3 verifies that the LEM extracted from this Gabor filters bank is better. We notice that when we increase ts, we lose the detailed information in vein

Table 4.6. MLHD measurement for double enrolment with different Gabor filters banks and LEM parameters.

		Gabor filters Bank Eq 3.13		**Gabor filters Bank Eq 3.14**		**Yuksel *et al.* [1]**
Set	**Rate**	**ts = 2**	**ts = 5**	**ts = 2**	**ts = 5**	**ts = 2**
Normal	IR	83.00	82.33	**85.66**	84.00	81.66
	EER	8.35	8.00	6.02	6.97	7.41
Activity	IR	86.11	83.66	**88.33**	85.00	86.66
	EER	7.23	7.77	6.42	7.33	6.47
Bag	IR	88.89	87.88	**89.00**	88.00	88.44
	EER	6.46	6.64	5.74	5.98	7.33
Ice	IR	80.88	79.22	**81.88**	79.66	80.77
	EER	9.67	10.01	8.92	8.56	9.13
All	IR	84.72	83.27	**86.21**	84.16	84.38
	EER	7.92	8.15	6.75	7.21	7.58

segments. This causes lower success rates for both identification and verification modes.

By comparing these results with the results from [1], we see that the performance is increased, except for the bag subset. It is possible to say that, "carrying bag" condition makes the veins more visible than other conditions. When a Gabor filter bank is also applied to this subset, the number of line segments of "carrying bag" condition LEMs becomes maximum. Having lots of line segments in a LEM decreases the efficiency of line segment based similarity measurement techniques. Because of this, the success rates of these methods are decreased.

Based on these results, we use Gabor filters bank as in Equation 3.14 and LEM with thin slope $ts = 2$ for enhancement in the rest of the experiments.

4.3.1.3. Experiment 3: Weighted LHD. An enhanced hand vein ROI consists of several vein segments in different intensity values. At first glance, these intensity values lead us to think that stronger vein segments play decisive roles on hand vein recognition. In order to understand this, we define a new MLHD metric, WLHD which evaluates the similarity scores by considering intensity values as weights. WLHD method and

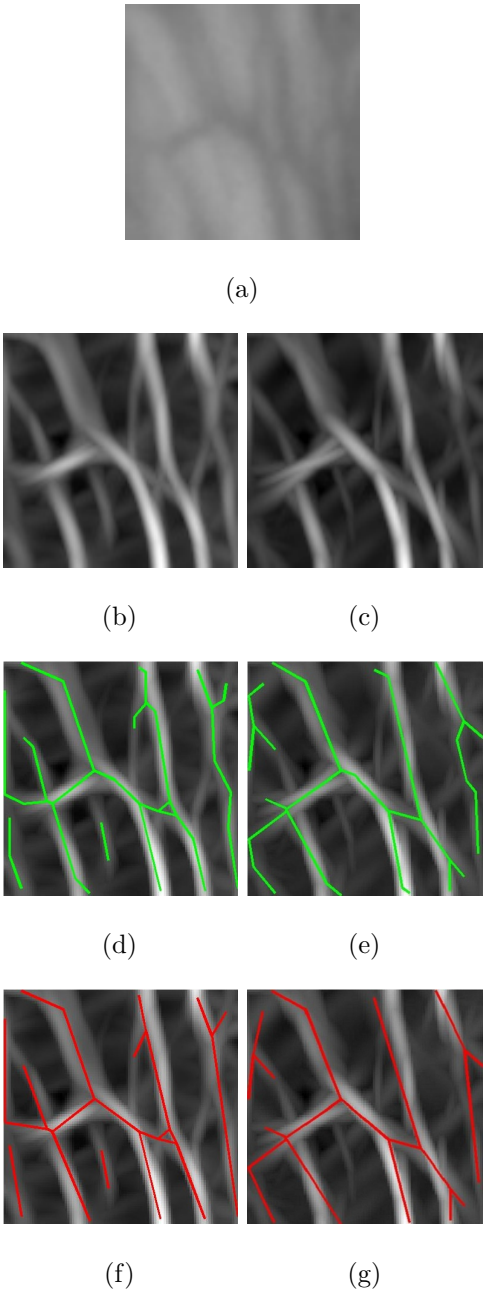

(a)

(b) (c)

(d) (e)

(f) (g)

Figure 4.3. Enhanced ROIs and their LEM forms constructed by different Gabor filters banks and parameters: (a) raw hand vein ROI, (b) Enhanced ROI extracted with (Equation 3.14), (c) Enhanced ROI extracted with (Equation 3.13), (d)LEM of enhanced ROI (b), with $ts = 2$, (e) LEM of enhanced ROI (c) with $ts = 2$ (f) LEM of enhanced ROI (b), with $ts = 5$, (g) LEM of enhanced ROI (c), with $ts = 5$.

the effects of weight parameters are discussed in Section 3.4.6 in detail. By selecting different weight parameters, WLHD based similarity matching is experimented and the results are demonstrated in Table 4.7 and Table 4.8, respectively.

We experiment with WLHD similarity matching by selecting different values for a and b parameters. Weighted LEM results show us that $a = 0.50$, $b = 5$ and $a = 0.60$, $b = 5$ parameter setups give better results than other parameter setups. If $a = 0, b = 1$ parameter set is used on line weights calculation (Equation 3.34), assigned weights are set in the range 0 to 1. For $a = 0.50$, $b = 5$ and $a = 0.60$, $b = 5$ parameter sets, this range converges to 0.9 to 1. It is easy to see that the influence of the weights decreases when the difference between the weights lessens.

Our conjecture about intensity values of vein segments was that, weak hand vein segments had lesser role than stronger ones in recognition. However, these results show us that weak vein segments provide improvement on identity matching as opposed to our conjecture.

4.3.1.4. Experiment 4: Iterative LEM. The test results in Table 4.5 demonstrate that Gabor filtering has the potential to improve vein structure visibility problems. However, there still exist problems caused by incorrect ROI extraction. Enhancing ROIs by evaluating their mean intensity values (as explained in Section 3.2.3 in detail) solves these problems to some extent but not entirely. We test iterative LEM construction method for this purpose. In order to measure the similarity score between two iterated LEMs, MLHD and LHD metrics are used. The results for single and double enrolment sets are given in Table 4.9 and Table 4.10.

Iterative LEM method considerably increases the success rate of the system. While iterating two ROIs, we align them as close as possible. Thus, the similarity score of registered ROIs improves. The first disadvantage of this method however is being dependent on the initial line segment. If it starts from a inaccurate line segment pair, we may not be able to register two ROIs. Second, iterative LEM construction

Table 4.7. WLHD measurement for single enrolment with different Gabor filters bank and WLHD parameter selections.

a	**Set**	**Rate**	**b=1**	**b=2**	**b=5**	**Gabor filters Bank Eq. 3.14**	**Yuksel *et al.* [1]**
0.60	Normal	IR	71.66	72.50	72.66	**73.00**	68.50
		EER	12.20	11.51	11.80	11.99	13.52
	Activity	IR	72.66	73.33	73.44	**74.33**	71.77
		EER	13.25	12.66	12.24	11.88	12.76
	Bag	IR	74.22	74.22	**74.55**	72.55	73.77
		EER	12.11	11.33	11.24	12.54	12.13
	Ice	IR	65.22	66.88	**67.11**	67.00	65.77
		EER	14.98	14.75	14.74	14.66	14.07
	All	IR	70.94	71.73	**71.92**	71.72	69.95
		EER	13.13	12.56	12.50	12.76	13.12
0.50	Normal	IR	70.33	72.33	72.66		
		EER	12.50	11.68	11.66		
	Activity	IR	70.88	73.22	73.44		
		EER	13.53	12.88	12.32		
	Bag	IR	73.66	74.00	74.66		
		EER	12.24	11.76	11.09		
	Ice	IR	64.33	66.55	67.00		
		EER	15.31	14.88	14.44		
0.35	Normal	IR	68.33	71.83	72.66		
		EER	14.08	12.35	11.66		
	Activity	IR	68.55	72.44	73.33		
		EER	14.21	13.22	12.42		
	Bag	IR	72.66	74.00	74.77		
		EER	13.54	12.01	11.28		
	Ice	IR	61.88	65.11	66.88		
		EER	15.98	15.10	14.57		
0.25	Normal	IR	66.16	70.33	72.66		
		EER	15.69	12.52	11.66		
	Activity	IR	66.11	71.11	73.22		
		EER	15.03	13.55	12.78		
	Bag	IR	70.88	73.66	74.00		
		EER	14.33	12.11	11.35		
	Ice	IR	59.88	64.66	66.77		
		EER	16.88	15.20	14.78		

Table 4.8. WLHD measurement for double enrolment with different Gabor filters bank and WLHD parameter selections.

a	**Set**	**Rate**	**b=1**	**b=2**	**b=5**	**Gabor filters Bank Eq. 3.14**	**Yuksel *et al.* [1]**
0.60	Normal	IR	85.00	85.00	85.33	**85.66**	81.66
		EER	6.44	6.71	6.30	6.02	7.41
	Activity	IR	87.88	88.33	**88.55**	88.33	86.66
		EER	6.46	6.31	6.33	6.42	6.47
	Bag	IR	**89.33**	**89.33**	**89.33**	89.00	88.44
		EER	5.65	5.47	5.66	5.74	7.33
	Ice	IR	80.77	**81.88**	**81.88**	**81.88**	80.77
		EER	8.78	8.90	8.88	8.92	9.13
	All	IR	85.89	86.13	**86.27**	86.21	84.38
		EER	6.83	6.84	6.79	6.75	7.58
0.50	Normal	IR	85.66	85.33	85.33		
		EER	7.13	6.71	6.41		
	Activity	IR	86.11	88.00	88.66		
		EER	6.99	6.20	6.23		
	Bag	IR	88.44	89.66	89.33		
		EER	6.34	5.43	5.55		
	Ice	IR	79.22	81.33	81.44		
		EER	8.88	8.99	8.87		
0.35	Normal	IR	83.33	85.00	85.00		
		EER	8.38	6.65	6.66		
	Activity	IR	83.55	87.77	88.22		
		EER	8.11	6.62	6.20		
	Bag	IR	86.66	89.44	89.44		
		EER	7.00	5.59	5.55		
	Ice	IR	76.11	80.33	81.55		
		EER	10.10	8.78	9.00		
0.25	Normal	IR	80.33	85.33	85.66		
		EER	9.36	7.25	6.92		
	Activity	IR	80.66	85.33	87.88		
		EER	8.77	6.97	6.20		
	Bag	IR	85.33	86.33	89.33		
		EER	8.23	6.30	5.45		
	Ice	IR	73.00	79.22	82.00		
		EER	11.47	8.98	8.99		

Table 4.9. LHD and MLHD measurements for single enrolment on iterated LEMs.

Set	**Rate**	**MLHD**	**LHD**	**Gabor filters Bank Eq. 3.14**	**Yuksel *et al.* [1]**
Normal	IR	75.5	**76.5**	73.00	68.50
	EER	9.70	10.29	11.99	13.52
Activity	IR	**80.11**	79.55	74.33	71.77
	EER	9.78	9.97	11.88	12.76
Bag	IR	82.44	**83.44**	72.55	73.77
	EER	8.35	7.89	12.54	12.13
Ice	IR	74.55	**75.22**	67.00	65.77
	EER	11.87	11.43	14.66	14.07
All	IR	78.15	**78.67**	71.72	69.95
	EER	9.91	9.89	12.76	13.12

Table 4.10. LHD and MLHD measurements for double enrolment on iterated LEMs.

Set	**Rate**	**MLHD**	**LHD**	**Gabor filters Bank Eq. 3.14**	**Yuksel *et al.* [1]**
Normal	IR	88.33	**89.66**	85.66	81.66
	EER	4.34	4.59	6.02	7.41
Activity	IR	**93.22**	93.11	88.33	86.66
	EER	3.90	4.32	6.42	6.47
Bag	IR	94.11	**94.33**	89.00	88.44
	EER	4.22	3.88	5.74	7.33
Ice	IR	86.44	**87.55**	81.88	80.77
	EER	7.01	6.79	8.92	9.13
All	IR	90.52	**91.16**	86.21	84.23
	EER	4.86	4.89	6.75	7.58

takes relatively more run time than simple LEM construction.

For normal, bag and ice test sets, LHD gives better results than MLHD. The only difference between MLHD and LHD measurement is seen on parallel distance measurement method. LHD calculates parallel distances between two segments more strictly than MLHD. Because of this, LHD can catch small differences in between parallel lines better. This becomes an advantage for correctly registered images, hence LHD works better for iterated LEMs.

4.3.1.5. Experiment 5: Keypoints. The results of the iterative LEM construction method show us that correctly registered ROIs increase success rate in both identification and verification modes. However, iterative LEM construction increases the runtime cost relatively. Due to this fact, we try to find another method which correctly registers the ROIs but does not increase runtime cost. For this purpose, we prefer to use keypoint matching and align ROIs based on matched keypoints. These keypoints can be junction points of the hand vein LEM or SURF detected interest points of an enhanced ROI. To extract descriptors from each keypoint type, the SURF interest point descriptor is employed. The effects of each keypoint type on recognition rates are compared in Table 4.9.

While aligning ROIs, using SURF interest points give better results than junction points. The main reason of this difference is that while constructing hand vein LEM of an enhanced ROI, the vein lines skeletonize the vein segments as fairly as possible. In fact, the intersection of vein segments gives us an area rather than an exact point. Because of this, in the course of junction points matching, we may be getting the real vein intersection areas but as the junctions cannot exactly define this area, they may not be matched. Moreover, a vein segment changes the intensity value of its near surfaces. Due to this, they do not have sharp edges. Since the SURF descriptor is designed for describing corner points of the image and the junctions do not fit the corner points, they may not be described efficiently.

Table 4.11. MHLD measurement for single enrolment on aligned ROIs using SURF interest points and junctions.

Set	**Rate**	**Junctions**	**SURF interest points**
Normal	IR	20.83	**50.83**
	EER	40.50	17.84
Activity	IR	21.11	**52.00**
	EER	40.91	25.21
Bag	IR	23.88	**51.55**
	EER	38.72	24.97
Ice	IR	16.44	**37.66**
	EER	41.76	32.03
All	IR	20.56	**48.01**
	EER	40.47	48.01

Furthermore, it is inevitable that SURF interest points lead to the matching of unrelated keypoints. Wrong matchings result in an incorrect alignment that reduces the intraclass similarity. So, bearing all these observations in mind, we design a condition statement which measures the similarity of two ROIs before and after alignment and then accepts the minimum one. The similarity scores are measured by MLHD and LHD methods, respectively. Table 4.12 show and Table 4.13 show the result of this combined method. As in Experiment 5, SURF based interest point matching and LHD similarity method will give more promising results as we expect.

Furthermore, we want to test whether we can use only keypoint matching for identity recognition or not. The similarity score is calculated by two methods. Firstly, we compare two ROIs on the basis of minimum distance between one of their matched keypoints. Secondly, we compare them by the number of matched keypoints. Table 4.14 demonstrates the results of this method.

The above mentioned negative effects of SURF interest points and junctions are

Table 4.12. MLHD and LHD measurement for single enrolment by accepting the minimum distance of aligned and not-aligned LEMs.

Keypoint Type	**Set**	**Rate**	**MLHD**	**LHD**	**Gabor filters Bank Eq. 3.14**	**Yuksel *et al.* [1]**
SURF interest points	Normal	IR	**77.5**	76.16	73.00	68.50
		EER	10.17	10.83	11.99	13.52
	Activity	IR	76.44	**76.66**	74.33	71.77
		EER	11.01	10.74	11.88	12.76
	Bag	IR	78.88	**80.55**	72.55	73.77
		EER	9.99	9.70	12.54	12.13
	Ice	IR	69.44	**70.55**	67.00	65.77
		EER	13.68	13.27	14.66	14.07
	All	IR	75.56	**75.97**	71.72	69.95
		EER	11.21	11.13	12.76	13.12
Junctions	Normal	IR	74.33	73.16		
		EER	11.49	11.66		
	Activity	IR	74.22	74.11		
		EER	12.33	11.78		
	Bag	IR	75.66	77.66		
		EER	11.43	10.12		
	Ice	IR	68.11	68.88		
		EER	14.35	13.56		
	All	IR	73.08	73.45		
		EER	12.40	11.78		

Table 4.13. MLHD and LHD measurement for double enrolment by accepting the minimum distance of aligned and not-aligned LEMs.

Keypoint Type	**Set**	**Rate**	**MLHD**	**LHD**	**Gabor filters Bank**	**Yuksel *et al.***
SURF interest points	Normal	IR	**88.66**	88.33	85.66	81.66
		EER	5.00	4.75	6.02	7.41
	Activity	IR	91.22	**91.11**	88.33	86.66
		EER	4.99	4.77	6.42	6.47
	Bag	IR	92.44	**93.22**	89.00	88.44
		EER	4.55	4.26	5.74	7.33
	Ice	IR	84.22	**84.33**	81.88	80.77
		EER	7.88	7.99	8.92	9.13
	All	IR	89,13	**89.24**	86.21	84.23
		EER	5,60	5,44	6.75	7.58
Junctions	Normal	IR	87.33	86.66		
		EER	5.67	5.66		
	Activity	IR	89.33	89.22		
		EER	5.66	5.58		
	Bag	IR	90.22	91.22		
		EER	5.01	5.24		
	Ice	IR	82.66	82.44		
		EER	8.35	8.53		
	All	IR	87.35	**87.38**		
		EER	6.17	6.25		

Table 4.14. The results of using keypoint matching for object recognition for single enrolment.

Keypoint Type	**Set**	**Rate**	**min dist based**	**max # matches**
SURF interest points	Normal	IR	**53.16**	31
		EER	17.63	70.14
	Activity	IR	**55.77**	34.11
		EER	15.59	72.77
	Bag	IR	**56**	39.88
		EER	16.02	73.74
	Ice	IR	**37.44**	23.22
		EER	20.52	68.49
Junctions	Normal	IR	28.5	10.5
		EER	30.97	61.71
	Activity	IR	28.44	9
		EER	29.03	61.01
	Bag	IR	28.55	9.11
		EER	29.52	61.22
	Ice	IR	18.77	5.66
		EER	34.66	58.62

manifested in low IR and high EER rates in Table 4.12. Besides, since each vein line segment has a limited feature combination set as orientation, scale, spatial information, etc., it is possible to find a very similar vein segment in two different person's ROIs. Thus, the idea in hand vein recognition has to be looking at the whole vein structure rather than individual interest points. On account of these, using only keypoints for recognition does not give us promising results.

4.3.1.6. Experiment 6: Matching by GED. All of the above mentioned experiments test hand vein LEMs by comparing the similarities between vein segments. We attempt to apply a different similarity score measuring method in this experiment. GED, which is mentioned in Section 3.4.7 is an alternative metric for measuring the similarities between two hand vein LEMs. The recognition results of this metric is shown in Table 4.15.

Table 4.15. GED measurement for single enrolment with different Gabor filter banks and LEM parameters.

		Gabor Filter Bank Eq. 3.14		**Gabor Filter Bank Eq. 3.13**	
Set	**Rate**	**ts = 2**	**ts = 5**	**ts = 2**	**ts = 5**
Normal	IR	**33.66**	30.33	30.83	27.33
	EER	23.80	27.30	28.18	29.12
Activity	IR	**34.44**	30.00	27.66	24.77
	EER	24.59	26.84	28.35	29.60
Bag	IR	**34.11**	31.22	31.44	26.77
	EER	25.05	25.92	27.86	28.97
Ice	IR	**26.33**	21.55	22.77	19.44
	EER	28.67	29.31	30.07	33.57

GED does not work as successfully as line segment based similarity methods. There are three main reasons of this:

(i) While measuring GED between two graphs, GED similarity metric measurement

algorithm visits vertices and calculates a similarity score based on whether these vertices are homologous on the other graph, or not. This depends strictly on the initial assignment. Matching junctions is more feasible than matching vertices. Nevertheless, angle similarity measurement that GED algorithm applies does not give promising matching results. This matching method decreases the success rate; however, finding a more appropriate junction matching method may not increase the results as much as we expect due to the impacts of the below mentioned causes.

(ii) External factors such as illumination and shape of the captured hand, affect the visibility of hand vein patterns in an hand vein image. This causes broken vein line segments in a graph. GED can not realize these broken line segments and tries to fill their positions which causes a cost. In other words, loss of only one vertex (node) misleads the algorithm and the similarity score between two hand vein vertices are calculated wrongly.

(iii) The factors affecting visibility of veins may also influence the number of vein lines which depict a vein segment. For example, a vein segment may be represented as two broken vein lines in a graph whereas it can be represented with only one in another. This causes troubles on GED calculation. In the course of node visiting, algorithm can not correlate that two lines in graph A and one line in graph B represent the same segment.

4.3.1.7. Conclusion. We have applied six different experiments on hand vein images both for identification and verification. So, bearing all these experiments in mind we reach two main inferences. First, Gabor filter bank is a very effective method to enhance apparency of vein segments on dorsal hand vein images. Last but not least, ineffective registration is the most significant problem of free-form captured hand vein images. We apply two methods, namely keypoint-based alignment and iterative LEMs to correct it. Correction on alignment yields more promising results than non-aligned ones.

Table 4.16 and Table 4.17 compare the three most successful results of experi-

ments with the literature [1].

Table 4.16. The most successful results of three experiments for single enrolment are compared to literature [1].

Set	**Rate**	**Iterative LEM**	**Keypoint**	**Gabor filters Bank Eq. 3.14**	**Yuksel *et al.* [1]**
Normal	IR	**76.50**	76.16	73.00	68.50
	EER	10.29	10.83	11.99	13.52
Activity	IR	**79.55**	76.66	74.33	71.77
	EER	9.97	10.74	11.88	12.76
Bag	IR	**83.44**	80.55	72.55	73.77
	EER	7.89	9.70	12.54	12.13
Ice	IR	**75.22**	70.55	67.00	65.77
	EER	11.43	13.27	14.66	14.07
All	IR	**78.67**	75.97	71.72	69.95
	EER	9.89	11.13	12.76	13.12

Table 4.17. The most successful results of three experiments for double enrolment are compared to literature [1].

Set	**Rate**	**Iterative LEM**	**Keypoint**	**Gabor filters Bank Eq. 3.14**	**Yuksel *et al.* [1]**
Normal	IR	**89.66**	88.33	85.66	81.66
	EER	4.59	4.75	6.02	7.41
Activity	IR	**93.11**	91.11	88.33	86.66
	EER	4.32	4.77	6.42	6.47
Bag	IR	**94.33**	93.22	89.00	88.44
	EER	3.88	4.26	5.74	7.33
Ice	IR	**87.55**	84.33	81.88	80.77
	EER	6.79	7.99	8.92	9.13
All	IR	**91.16**	89.24	86.21	84.38
	EER	4.89	5.44	6.75	7.58

5. CONCLUSIONS

5.1. Conclusion and Future Work

In this thesis, we propose several methods to be used in different stages of a geometry-based biometric system for recognizing identities through their free-posture captured hand vein images. A hand vein biometric system is composed of four significant steps, namely, image acquisition, Region of Interest (ROI) extraction, feature extraction, and identity matching. We use Bosphorus Hand Vein Database for enrolment and test. This database consists of free-posture hand vein images captured with NIR cameras. As a hand vein image covers an entire hand, the ROI encapsulating the hand vein structure has to be extracted. We use Yoruk Algorithm for ROI extraction. Yoruk algorithm finds finger valleys and selects the ROI by employing these valley points. Position of the fingers is a substantial factor in determining the location of finger valleys. If fingers are quite close to each other, finger valleys may be detected inaccurately. Inaccurately detected finger valleys cause ROIs to be incorrectly extracted. The best way to prevent incorrect ROI extraction is to work on a database captured under controlled conditions. But if free-posture captured database has to be used, there is not a certain way to inhibit incorrect registration. Therefore, biometrics that work on free-posture captured images have to use algorithms robust to incorrect ROIs. For future work, we plan to make our algorithms more robust to registration errors. In addition to this, we intend to investigate registration techniques more deeply. We will analyse whether to extract keypoints from hand vein structures, and then utilize them for registration as an alternative to finger valleys.

In this thesis we propose two separate ROI correction approaches to meliorate inaccurately extracted ROIs. Mean intensity technique is based on the following observation: Incorrect ROIs hold irrelevant information, usually like finger valleys or wrist area. As these extraneous regions are darker than hand vein area, a ROI that holds irrelevant information has lower mean intensity values than correct ones. Hence, we design an algorithm that determines incorrect ROIs by looking at their mean intensity

values. It attempts to crop incorrect ROIs from up and down sides to throw out any extraneous information on finger valleys or wrist area. After a visual inspection of corrected ROIs, we observe that the mean intensity based ROI correction approach serves the purpose to a certain extent.

Apart from this, we present another ROI correction approach which we call warping ROIs. Due to the movement of a hand, there could be some deformation; especially on the wrist area for dissimilar postures. In order to correct deformation by warping ROIs approach, we utilize the TPS (Thin Plate Spline) algorithm. TPS is an algebraic approach that maps two patterns. To do this, TPS deforms one pattern to another by transforming each pattern's selected landmarks. In our problem, we define landmarks as finger valleys for each hand segment. Afterwards, we map all hand segments to a model template to amend the deformed area. The model hand segment is represented by mean finger valleys that are measured by considering 100 truly normalized hand segments of 50 different subjects. Experiment 1 demonstrates that this approach impairs the vein structure much more, rather than correcting it. After a detailed investigation, we realize two factors. Firstly, hand segmentation algorithm cannot find finger locations accurately in all circumstances. Secondly, while using TPS warping, the farther the deformed area is to reference points, the less the effect of the change is observed. Since wrist area is far away to the finger valleys, warping operation does not correct the deformed area sufficiently. For these reasons, we do not apply this approach in our further experiments. Nevertheless, warping ROIs may be utilized more efficiently. For instance, the amount of warping deformation of two hand segments can guide us whether they belong to the same identity or not. For future work, we aim to investigate on warping deformation amounts and extract useful information to be used for identity recognition.

At feature extraction stage of this study, we extract features from corrected ROIs. Prior to feature extraction, we enhance vein visibility by Gabor filters banks. Usage of Gabor filters bank for this aim is a new thing for hand vein biometric literature. We use two different Gabor filters banks in this study. One of them is Yang *et al.*'s [26] Gabor filters bank which is used for finger vein enhancement. The second one is

standard Gabor filters bank that we propose to utilize for vein visibility enhancement. The main difference between these two banks is the DC elimination. The first filters bank eliminates DC response whereas the second one does not. Experiment 2 indicates that the latter bank works better than the former one. We are inclined to believe that, there are two basic reasons behind this. In the first place, our utilized hand vein database is collected in a dark room to eliminate the effects of visible light. Due to this fact, there is not a requisite for DC elimination while filtering the images. Beyond this, using a DC eliminating filter unnecessarily deforms the current hand vein structures. The second reason is that, the former filters bank is designed for finger vein patterns. Finger vein patterns are thinner and closer to each other than the hand vein ones. Pursuant to this, Yang *et al.*'s Gabor filters bank tends to separate a vein pattern into several, tiny partitions. This detailed and sensitive filter is not proper for a hand vein structure. Above all, we apply our proposed Gabor filters bank to ROIs and use new enhanced ROIs for further stages.

We use Yasuda binarization to extract hand vein structures from enhanced ROIs. Extracted hand vein patterns are skeletonized and converted into line segments by the Line Edge Map (LEM) method, respectively. Hand vein structures converted into line segments form graphs. The most important points on this process are as follows: Firstly, because Yasuda binarization method does not yield hand vein structures in a flawless manner, enhanced ROIs cannot be utilized sufficiently. Therefore, we intend to investigate more successful binarization methods and apply them in future works. Secondly, skeletonization of hand vein structures results in loss of superficialness and thickness property of a vein pattern. In order to avoid the loss to some extent, we modify Line Segment Hausdorff Distance (LHD) and propose Weighted LHD (WLHD) similarity metric. Nonetheless, proposing new methods which use physical properties of vein patterns much more than WLHD may be better for identity matching. We aim to work also on this direction as future work. The third important point is the line slope parameter selection of the LEM algorithm. LEM converts a vein pattern to several lines considering the selected line slope parameter. Selecting inaccurate slope parameter leads to extract vein line segments incompatible with the corresponding hand vein pattern. Experiment 2 shows that correct slope parameter increases the

recognition success rate dramatically.

As it is mentioned above, we achieve ROI correction to some extent by using their image properties. While matching identities, we notice that these corrections are not adequate for identity matching and registration errors still affect the success of the system greatly. Hence, we append a ROI coinciding module, as a postprocessing step, just before the similarity score calculation in identity matching stage. Postprocessing module endeavours to amend ROI registration by coinciding test and enrolled ROIs rather than correcting all ROIs independently. We propose two main techniques to be optionally used for superposing. The first technique relies on keypoint matching. It matches keypoints that are selected from test and enrolled ROIs, and reforms these ROIs by coinciding matched keypoint pairs. We use two different keypoint sets for this end. Firstly, we elect junction points, which are intersecting points of three or more vein lines, from LEMs and use them as keypoints. Secondly, we utilize interest point detector of Speeded Up Robust Features (SURF) to extract keypoints. SURF is a scale and rotation invariant interest point detector and descriptor. in image processing literature, there is another interest point detector and descriptor algorithm, Scale-invariant feature transform (SIFT), which is widely-used in biometric area. We observe these two detectors and do not notice substantial difference between both methods' coincided ROIs. As SURF has an advantage of run time cost over SIFT, we prefer to use SURF in further experiments.

After keypoint selection, we extract descriptions from keypoints by means of SURF interest point descriptor. Each keypoint is matched with corresponding keypoint of the compared ROI in accordance with their descriptions. A keypoint is paired with the most similar keypoint in the compared ROI where the similarity between two keypoints is calculated by Euclidean distance between their descriptiors. We compute the transformation function belonging to the compared ROIs with regrading keypoint pairs. Afterwards, we apply the transformation function on test ROI's hand vein graph to coincide test and enrolled graphs. However, we notice that compared graphs are incorrectly superposed in the case of inaccurate keypoint matching and thus the similarity between the two graphs inevitably decreases. To tolerate the effect of incorrectly

matched keypoint pairs, we find the similarity score as follows: The similarity score between the compared graphs are measured both before and after the coincidence. We fuse the results, by accepting the best one as the compared graphs' similarity score.

The results of Experiment 5 represent that employing SURF interest points as keypoints rather than junction points coincides compared graphs better. The most considerable factor of this result is based on the working principle of SURF interest point descriptor. SURF interest point descriptor is designed to describe corner points in an image. A junction point of a graph may not represent a corner point in the graph's corresponding ROI image. In such a case, SURF descriptor does not extract appropriate descriptions for these junction points. Consequently, SURF interest points provide more successful coincidence on graphs when compared with junction points. Experiment 5 also shows that fusing similarity scores which are calculated before and after graph coincidence, ensures better results rather than using only the coincided graphs.

The second superposing technique of the postprocessing module is called iterative LEM method. Iterative LEM method coincides test and enrolled hand vein graphs based on homologous vein lines. It superposes the most similar vein line pair belonging to compared graphs and transforms the test graph's line to enrolled one's direction. Subsequently, test graph is shifted towards the most similar vein line pair in an iterative manner. In each iteration, the similarity score between enrolled and test graphs are measured and the best one is admitted. Experiment 4 and 5 exhibit that both of these postprocessing methods increase the success rate dramatically. Iterative LEM approach has disadvantages as being strongly dependent on the reference vein line pair and additionally having higher runtime cost than keypoint matching. However, it improves the recognition success rate much more than the keypoint matching approach.

As it is mentioned in Section 4.2, a biometric recognition system works on two different modes; one is identification, the other is verification. Both of these modes utilize similarity score calculation to identify hand vein structures. Similarity score is used for making a decision whether compared hand vein structures originate from

the same individual or not. In this study, we work on graph forms of a hand vein structure in identification phase. We use four different graph and line distance measurement techniques to calculate similarity score between compared graphs. These are namely Line Segment Hausdorff Distance (LHD), Weighted Line Segment Hausdorff Distance (WLHD), Modified Line Segment Hausdorff Distance (MLHD) and Graph Edit Distance (GED) measurement techniques. LHD is a distance metric which describes distance between two lines in terms of angular, vertical and parallel distances. It is previously used in hand vein biometry literature. By modifying LHD, we propose two new LHD metrics named as WLHD and MLHD. MLHD is designed to tolerate registration errors. The only difference between LHD and MLHD metrics is seen when one line is the superset of the other. In that case, MLHD determines the parallel distance as zero. WLHD intends to enhance the impact of thicker and stronger hand vein segments on similarity score calculation, by giving coefficients to them. We apply the following way to calculate vein line coefficients: We construct a rectangle for each vein line segment which encapsulates the corresponding vein line. Thickness and strength of a vein segment can be realized by looking at the average intensity values in enhanced ROI. Thus, we determine a coefficient for each line according to the average intensity values of pixels inside the corresponding rectangle in the enhanced ROI. So as to regulate the coefficients, we form a two-parametrized function which makes the coefficients dependent on the parameters, as is given in Section 3.4.6, Equation 3.34.

In experiment 4 and 5, we compare the performances of MLHD and LHD measurement metrics. It is seen that MLHD works better than LHD on hand vein graphs on which no postprocessing method is applied. Two ROIs of the same hand vein structure may be incorrectly extracted and therefore some differences may occur in two ROIs. For example, a hand vein segment may be shifted or appears shorter or longer than it is. Since MLHD can tolerate this kind of problems more than LHD, it gives better results on hand vein structures that are not postprocessed. Experiment 3 demonstrates the effects of strong or weak vein segments on identification by using WLHD measurement metric. When visually inspecting hand vein ROIs, weak vein segments appear to have less impact on identification. Nevertheless, the results of experiment 3 shows that they provide improvement on identity matching as opposed to our hypothesis.

In addition to the line segment based similarity measurement techniques, we propose to employ GED similarity distance measurement for identifying graphs. Suppose that we have two graphs as G and G', GED is the least cost that is spent to simulate graph G to G'. It simulates graphs by employing six main operators namely node insertion, node deletion, node substitution, edge insertion, edge deletion and edge substitution. While attempting to simulate graph G to G', firstly initial vertex pairs are selected from both graphs. Then, both graphs are traversed and required operations are applied to graph G. At the final step, we gain homologous graphs and The least cost (GED) is calculated. An example to this simulation is given in Section 3.4.7.3.

GED is previously used for fingerprint classification. In this study, we modify this method to make it applicable for hand vein biometry. Experiment 6 reveals that GED measurement does not give promising success rates for recognition. When we examine the results, we notice that there is more than one reason. First, GED strictly depends on the initial vertices assignment. To determine initial assignment, we try to match junction points by considering their angular similarities. This matching method is one of the reasons of low success rates. But, a more suitable junction matching method may not significantly improve the GED results due to other reasons: Second major factor of low success rates is broken vein segments. A weak hand vein segment may not be discernible in a captured image. Presence of broken vein line segments in a hand vein graph may be therefore inevitable. Since GED calculation algorithm can not tolerate them, loss of only one vertex misleads the algorithm and causes gratuitous GED cost. Lastly, a vein segment may be depicted with different number of vein lines in different graphs and GED calculation algorithm cannot define that they belong to the same segment. It results in unnecessary operations which leads to increased GED cost.

For identity matching, we also attempt to match identities by considering the most similar keypoints or the amount of successful matches. While considering the most similar keypoints, we compare the current test ROI with all enrolled ROIs and keep the most similarly matched keypoint pairs. Then, test ROI is assigned to the enrolled ROI in which the closest keypoint match occurs. Secondly, we regard the

number of matched keypoints for each comparison and the current test ROI is assigned to the enrolled ROI where the highest number of matches occurs. Experiment 5 evinces that although the latter method works better than the former one, neither of them give promising results. Due to this, we realize that looking at the hand vein structure as a whole is therefore essential for hand vein biometry.

Hand vein recognition is a preferred biometric for several reasons: It is nonintrusive and easily collected; it permits liveness tests, it is hard to modify. Several methods have been proposed for identification based on hand veins. In this thesis, we have tested several geometry based techniques and concluded that registration is a crucial step and that global techniques are more successful. Future studies must concentrate on better registration and more successful vein segment extraction.

REFERENCES

1. Yüksel, A., L. Akarun and B. Sankur, "Hand Vein Biometry Based on Geometry and Appearance Methods", Vol. 5, 2011.

2. Editorial, "Hand-based Biometrics", *Biometric Technology Today*, Vol. 11, No. 7, pp. 9–11, 2003.

3. Badawi, A. M., "Hand Vein Biometric Verification Prototype: A Testing Performance and Patterns Similarity", *In Proceedings of the 2006 International Conference on Image Processing, Computer Vision, and Pattern Recognition*, Las Vegas,USA, 2006.

4. Jain, A. K. and A. A. Ross, *Handbook of Biometrics*, Springer, 2008.

5. Cross, J. and C. Smith, "Thermographic Imaging of The Subcutaneous Vascular Network of The Back of The Hand for Biometric Identification", *Security Technology, 1995. Proceedings. Institute of Electrical and Electronics Engineers 29th Annual 1995 International Carnahan Conference on*, pp. 20–35, 1995.

6. Tech-sphere, *The dependable biometrics Techsphere*, 2009, `http://tech-sphere.com/en/index.asp`, accessed at March 2012.

7. Wang, L., G. Leedham and S.-Y. Cho, "Infrared Imaging of Hand Vein Patterns for Biometric Purposes", *Computer Vision, IET*, Vol. 1, No. 3-4, pp. 113–122, 2007.

8. Lin, C. L. and K. C. Fan, "Biometric Verification Using Thermal Images of Palm-Dorsa Vein Patterns", *IEEE Transactions on Circuits and Systems for Video Technology*, Vol. 14, No. 2, pp. 199–213, 2004.

9. Wang, L., G. Leedham and D. S.-Y. Cho, "Minutiae Feature Analysis for Infrared Hand Vein Pattern Biometrics", *Pattern Recognition*, Vol. 41, No. 3, pp. 920–929,

2008.

10. Chen, L., H. Zheng, L. Li, P. Xie and S. Liu, "Near-Infrared Dorsal Hand Vein Image Segmentation by Local Thresholding Using Grayscale Morphology", *Bioinformatics and Biomedical Engineering, 2007. ICBBE 2007. The 1st International Conference on*, pp. 868–871, 2007.

11. Im, S.-K., H.-M. Park, S.-W. Kim, C.-K. Chung and H.-S. Choi, "Improved vein pattern extracting algorithm and its implementation", *Consumer Electronics, 2000. ICCE. 2000 Digest of Technical Papers. International Conference on*, pp. 2 –3, 2000.

12. Tanaka, T. and N. Kubo, "Biometric Authentication by Hand Vein Patterns", pp. 2–3, 2004.

13. Mohit, S., "A New Vein Pattern-Based Verification System", Vol. 8, pp. 58–63, 2010.

14. Xu, J., C. Jianjiang, X. Dingyu and P. Feng, "Near Infrared Vein Image Acquisition System Based on Image Quality Assessment", *Electronics, Communications and Control (ICECC), 2011 International Conference on*, pp. 922–925, 2011.

15. Wang, Y., K. Li, J. Cui, L.-K. Shark and M. Varley, "Study of Hand-Dorsa Vein Recognition", D.-S. Huang, Z. Zhao, V. Bevilacqua and J. Figueroa (Editors), *Advanced Intelligent Computing Theories and Applications*, Vol. 6215 of *Lecture Notes in Computer Science*, pp. 490–498, Springer Berlin / Heidelberg, 2010.

16. Heenaye, M. and N. Khan, "Low Dimensional Representation of Dorsal Hand Vein Features Using Principle Component Analysis (PCA)", Vol. 37, pp. 1091–1097, World Academy of Science, Engineering and Technology, Dubai, United Arabs Emirates, 2009.

17. Hsu, C.-B., S.-S. Hao and J.-C. Lee, "Personal Authentication through Dorsal

Hand Vein Patterns", Vol. 50, pp. 87201–87201, 2011.

18. Lu, W., X. Qi and C. Liu, "Fusion of Palm Dorsal Vein and Hand Geometry for Personal Identification Based on Linear Discriminant Analysis", *Proceedings of the 2010 Fifth International Conference on Frontier of Computer Science and Technology*, FCST '10, pp. 532–536, IEEE Computer Society, Washington, DC, USA, 2010.

19. Zhao, S., Y. Wang and Y. Wang, "Extracting Hand Vein Patterns from Low-Quality Images: A New Biometric Technique Using Low-Cost Devices", *Image and Graphics, 2007. ICIG 2007. Fourth International Conference on*, pp. 667–671, 2007.

20. Sezgin, M. and B. Sankur, "Survey over Image Thresholding Techniques and Quantitative Performance Evaluation", *Journal of Electronic Imaging*, Vol. 13, No. 1, pp. 146–168, 2004.

21. Wang, Y., D. Wang, T. Liu and X. Li, "Local SIFT Analysis for Hand Vein Pattern Verification", Vol. 7512, pp. 4–8, 2009.

22. Wang, H.-b., L. Tao and X.-y. Hu, "Novel Algorithm for Hand Vein Recognition Based on Retinex Method and SIFT Feature Analysis", X. Wan (Editor), *Electrical Power Systems and Computers*, Vol. 99 of *Lecture Notes in Electrical Engineering*, pp. 559–566, Springer Berlin Heidelberg, 2011.

23. Yörük, E., E. Konukoğlu, B. Sankur and J. Darbon, "Shape-Based Hand Recognition", *IEEE Transactions on Image Processing*, Vol. 15, No. 7, pp. 1803–1815, 2006.

24. Yörük, E., H. Dutağaci and B. Sankur, "Hand Biometrics", *Image Vision Computing*, Vol. 24, pp. 483–497, 2006.

25. Bookstein, F. L., "Principal Warps: Thin-Plate Splines and the Decomposition

of Deformations", *IEEE Trans. Pattern Anal. Mach. Intell.*, Vol. 11, No. 6, pp. 567–585, 1989.

26. Yang, J., J. Yang and Y. Shi, "Finger-Vein Segmentation Based on Multi-Channel Even-Symmetric Gabor Filters", *Intelligent Computing and Intelligent Systems, 2009. ICIS 2009. IEEE International Conference on*, Vol. 4, pp. 500–503, 2009.

27. Daugman, J. D., "Two-Dimensional Spectral Analysis of Cortical Receptive Field Profiles", *Vision Research*, Vol. 20, No. 10, pp. 847–856, 1980.

28. Daugman, J. D., "Uncertainty Relation For Resolution in Space, Spatial Frequency, and Orientation Optimized by Two-Dimensional Visual Cortical Filters", Vol. 2, pp. 1160–1169, 1985.

29. Lee, T. S., "Image Representation Using 2D Gabor Wavelets", *IEEE Transactions Pattern Analysis and Machine Intelligence*, Vol. 18, pp. 959–971, 1996.

30. Movellan, J. R., *Tutorial on Gabor Filters*, Tech. rep., MPLab Tutorials, Univ. of California, San Diego, 2008.

31. Kamarainen, J.-K., V. Kyrki and H. Kalviainen, "Invariance Properties of Gabor Filter-Based Features-Overview and Applications", *Image Processing, IEEE Transactions on*, Vol. 15, No. 5, pp. 1088–1099, 2006.

32. Yüksel, A., L. Akarun and B. Sankur, "Biometric Identification through Hand Vein Patterns", *Emerging Techniques and Challenges for Hand-Based Biometrics (ETCHB), 2010 International Workshop on*, pp. 1–6, 2010.

33. Gao, Y. and M. Leung, "Face Recognition Using Line Edge Map", *Pattern Analysis and Machine Intelligence, IEEE Transactions on*, Vol. 24, No. 6, pp. 764–779, 2002.

34. Gower, J. C., "Generalized Procrustes Analysis", Vol. 40, No. 1, pp. 33–51, 1975.

35. Goodall, C., "Procrustes Methods in Statistical Analysis of Shape", Vol. 53, No. 2,

pp. 285–339, 1991.

36. Bay, H., T. Tuytelaars and L. V. Gool, "SURF: Speeded Up Robust Features", *In ECCV*, pp. 404–417, 2006.

37. Bay, H., A. Ess, T. Tuytelaars and L. Van Gool, "Speeded-Up Robust Features (SURF)", *Comput. Vis. Image Underst.*, Vol. 110, No. 3, pp. 346–359, Jun. 2008.

38. Gao, X., B. Xiao, D. Tao and X. Li, "A Survey of Graph Edit Distance", *Pattern Analysis and Applications*, Vol. 13, pp. 113–129, 2010.

39. Neuhaus, M. and H. Bunke, "An Error-Tolerant Approximate Matching Algorithm for Attributed Planar Graphs and Its Application to Fingerprint Classification", *In: Proc. 10th Int. Workshop on Structural and Syntactic Pattern Recognition. LNCS 3138*, pp. 180–189, Springer, 2004.

40. Ambauen, R., S. Fischer and H. Bunke, "Graph Edit Distance with Node Splitting and Merging, and Its Application to Diatom Identification", E. Hancock and M. Vento (Editors), *Graph Based Representations in Pattern Recognition*, Vol. 2726 of *Lecture Notes in Computer Science*, pp. 259–264, Springer Berlin/Heidelberg, 2003.

41. Frangi, A. F., W. J. Niessen, K. L. Vincken and M. A. Viergever, "Multiscale Vessel Enhancement Filtering", G. Goos, J. Hartmanis and J. van Leeuwen (Editors), *Proc Intern Conf on Medical Image Computing and Computer-Assisted Intervention (MICCAI)*, Vol. 1496 of *LNCS*, pp. 130–137, Springer, Cambridge, MA, 1998.

42. Wang, Y., T. Liu and J. Jiang, "A multi-resolution wavelet algorithm for hand vein pattern recognition", *Chin. Opt. Lett.*, Vol. 6, No. 9, pp. 657–660, Sep 2008.

43. Zhang, D., Z. Guo, G. Lu, L. Zhang and W. Zuo, "An online system of multispectral palmprint verification", *Instrumentation and Measurement, IEEE Transactions on*, Vol. 59, No. 2, pp. 480–490, 2010.